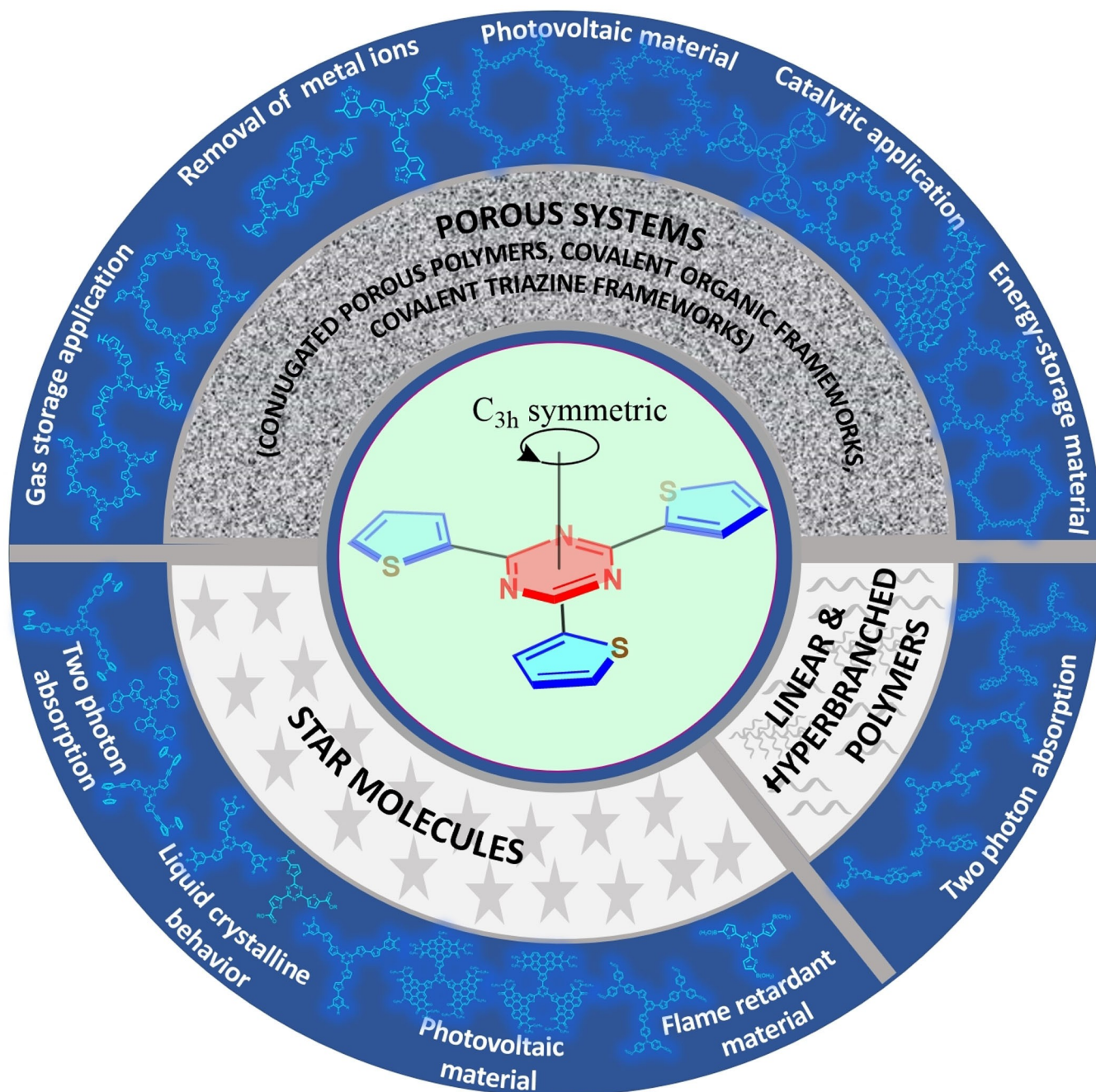


Advances in the Chemistry of 2,4,6-Tri(thiophen-2-yl)-1,3,5-triazine

Neha Rani Kumar^{*[a]} and Abhijeet R. Agrawal^[b]



Heterocyclic systems are now considered to be an integral part of material chemistry. Thiophene, selenophene, furan, pyrrole, carbazole, triazine and others are some such examples worth mentioning. 2,4,6-Tri(thiophen-2-yl)-1,3,5-triazine is a C_{3h} -symmetric system with thiophene as the donor unit and *s*-triazine as the acceptor unit. This review gives an insight into the advances made in the thienyl-triazine chemistry over the past

two to three decades. The synthetic pathways for arriving at this system and all its important derivatives are provided. The major focus is on the materials synthesized using the thienyl-triazine system, including star molecules, linear and hyperbranched polymers, porous materials and their diverse applications. This review will play a catalytic role for new dimensions to be explored in thienyl-triazine chemistry.

1. Introduction

Materials science is an interdisciplinary field that has emerged by bridging the gap between physics, chemistry, biology and allied fields. The last three decades have led to significant achievements in material chemistry. Both organic and inorganic compounds have contributed significantly in this regard. Organic compounds have been the trend setter to achieve new heights in the field of organic semiconductors, biomaterials, liquid crystals etc. The mention of heterocycles cannot be ignored in this regard and heterocyclic chemistry has led to immense contribution and ground-breaking results for an overall progress of material science.^[1] Amongst the wide class of heterocycles available, thiophene, selenophene, carbazole, pyrrole, furan, pyridine, triazine etc. are some systems that have played a key role for the wide application of organic compounds in material chemistry.^[2]

Thiophene is a heterocycle with the formula C_4H_4S and consists of one sulfur as heteroatom.^[3] The versatile applications of thiophene based compounds emerge from several contributing factors such as its easy and inexpensive availability as a by-product of petroleum distillation, easy functionalization of α - and β - positions of thiophene, easy synthesis of thiophene based regioregular molecules and polymers, easy synthesis of wide class of materials like linear systems, branched systems, star shaped systems and dendrimers and their stability etc.^[4–16] All these factors further contribute in establishing a detailed structure property relationship by fine tuning of the materials.^[17]

Triazine is another important heterocycle that consists of three nitrogen atoms, i.e., a system in which three carbon-hydrogen units in benzene are replaced by nitrogen. There are three isomers of triazine depending on the position of the nitrogen atoms. These isomers are 1, 2, 3-triazine (asymmetrical triazine or vicinal triazine 1.1), 1, 2, 4-triazine (asymmetrical triazine or isotriazine 1.2) and 1, 3, 5-triazine (symmetrical or *s*-

triazine or cyanidine 1.3) (Scheme 1A).^[18] Triazine based systems have also been of immense biological significance.^[19,20] The symmetric triazine isomer, that is, 1,3,5-triazine also referred as *s*-triazine (1.3) is the most interesting and important isomer that has been used in variety of applications. The importance of *s*-triazine in material chemistry can be attributed mainly to its high electron affinity, symmetry and different type of supramolecular interactions that it gives rise to. This system has huge potential for formation of different types of non-covalent bonds (Scheme 1B) that involve either nitrogen lone-pairs (H-bonds and coordination), heteroaromatic π -electrons (π - π stacking and cationic- π interactions) or its σ backbone (anionic- σ and electron rich- σ interactions).^[21–26]

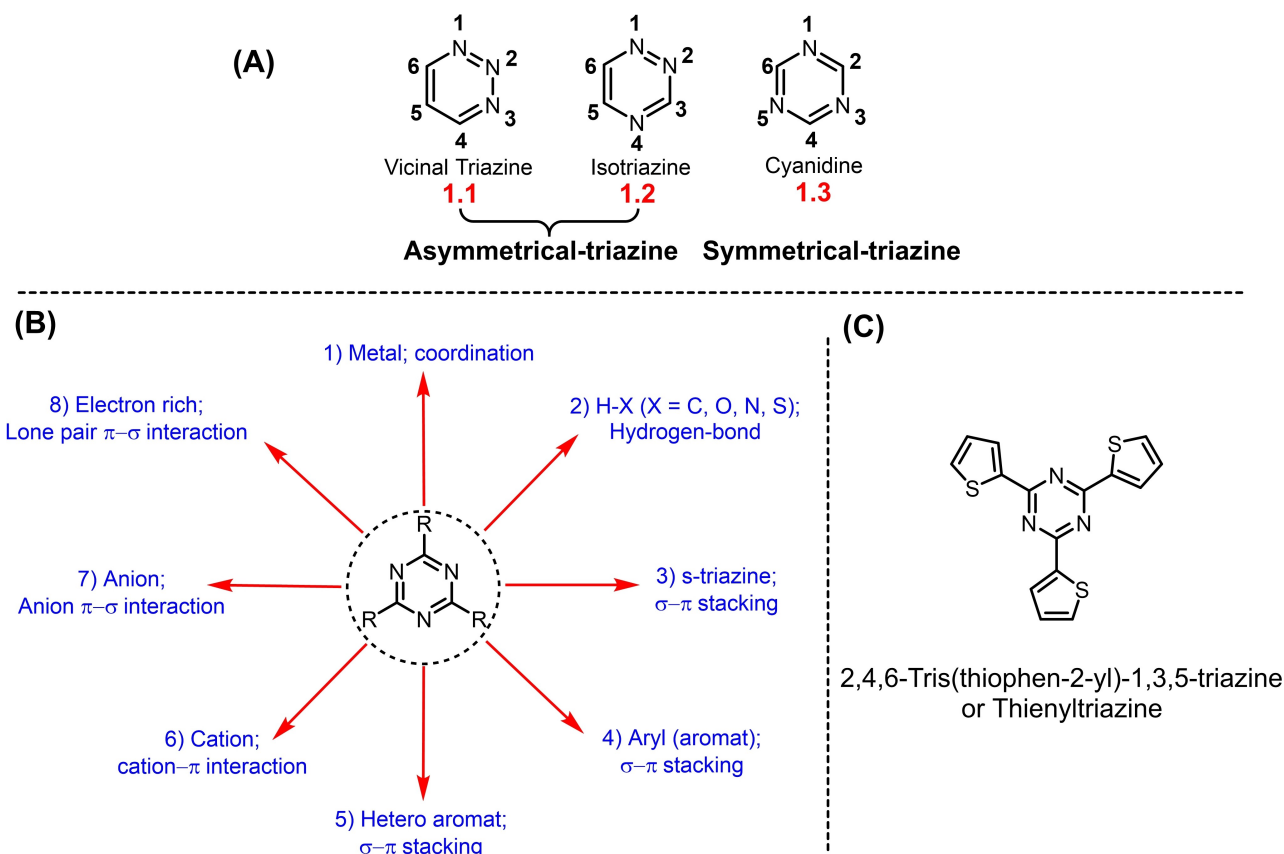
Undoubtedly if there is a system that involves both thiophene and the triazine unit, it is expected to show interesting properties and act as a foundation for diverse class of materials with intriguing applications in material chemistry. An interesting example of this class of material is 2,4,6-Tri(thiophen-2-yl)-1,3,5-triazine (Scheme 1C). This molecule possesses unique features such as a π -electron deficient core that is 1,3,5-triazine, three thiophene as π -electron rich side branch, highly symmetrical and coplanar structure (C_{3h} symmetry), possibility of easy functionalization of α -positions of thiophene for further extension of conjugation etc. Both the thiophene and triazine units can lead to different types of interaction in the resulting compounds.^[27] Presence of thiophene has been known to enhance intra- and intermolecular interactions such as Vander Waals interaction, π - π stacking, weak hydrogen bonds, S...S interactions arising due to the high polarizability of the presence of sulfur.^[28–30] As discussed previously, triazine unit enhances the existence of supramolecular interactions. The incorporation of thienyltriazine in material chemistry leads to compounds with narrow energy gap (band gap) which means the structural and optical properties of the resulting materials can be easily tuned by tuning the extent of conjugation of the groups present.^[27]

Also, molecules with strong pull-push effect (donor-acceptor) and good coplanarity enhance the flow of electrons and/or holes and also facilitate exciton separation. Large number of heteroatoms also widen the possibility of interaction with guest molecules. These all-contributing factors have made thienyltriazine a very interesting candidate that has been explored in diverse fields like organic electronics, porous organic chemistry etc. Such donor-acceptor systems have been used for the synthesis of star type systems, linear polymers, porous materials and such systems have been known to show two-photon absorption behaviour, catalytic behaviour, energy storage

[a] Dr. N. Rani Kumar
Department of Chemistry Dhemaji College
Dhemaji, 787057, Assam, India
E-mail: nehakumar0926@gmail.com

[b] Dr. A. R. Agrawal
Institute of Chemistry
The Hebrew University of Jerusalem
Edmond J. Safra Campus, Jerusalem, 91904, Israel

 © 2023 The Authors. Published by Wiley-VCH GmbH. This is an open access article under the terms of the Creative Commons Attribution Non-Commercial License, which permits use, distribution and reproduction in any medium, provided the original work is properly cited and is not used for commercial purposes.



Scheme 1. (A) Structural isomers of triazine (B) Potential supramolecular interactions of the s-triazine ring involving 1–2), the nitrogen lone pairs; 3–6), the heteroatomic π electrons; and 3–5) and 7–8), the σ backbone. Reproduced with permission from Ref. [21], Copyright Elsevier, 2007. (C) Structure of Thienyltriazine.

property, and have been used in CO₂ sequestration, catalytic behaviour, liquid crystalline behaviour and more.^[28–44]

Though a unique and interesting system, thienyltriazine chemistry is yet to be explored to obtain the best out of it. This review is intended to serve this purpose and here we have summarized the major advances that have taken in the thienyltriazine chemistry over the span of past two-three decades. This includes insights into the synthesis of thienyltriazine and its important functionalised derivatives. The major focus is on the application of thienyltriazine system for the synthesis of star molecules, linear and hyperbranched polymers and porous materials. At the end we have discussed some

challenges that need to be addressed for further research in this direction.

2. Synthesis of Thienyltriazine and its Derivatives

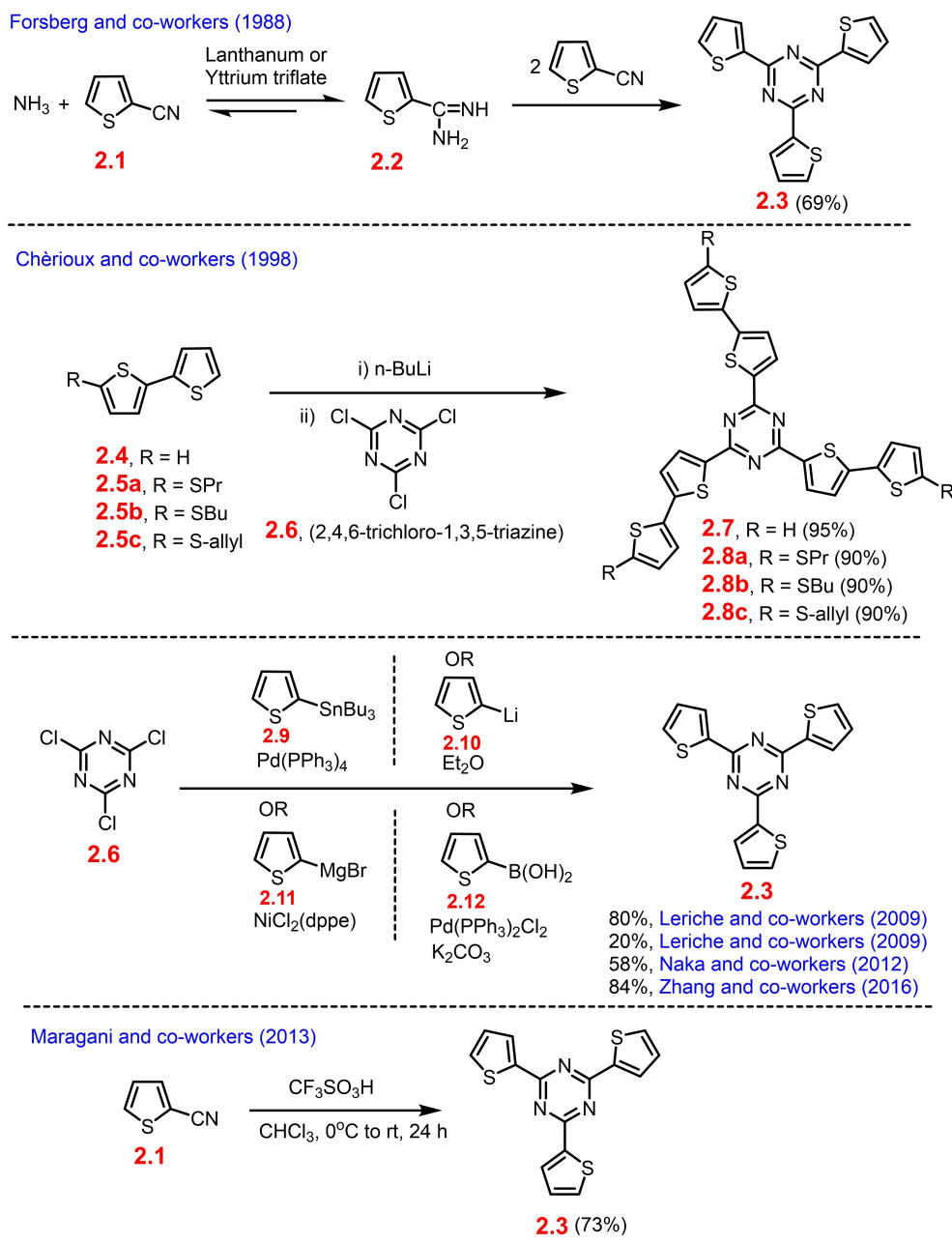
Important synthesis methods of 2,4,6-tri(thiophen-2-yl)-1,3,5-triazine and its functionalized derivatives that act as precursors for the synthesis of wide array of materials are outlined in Scheme 2.



Neha Rani Kumar received her M.Sc. degree in Chemistry from Gauhati University, India in 2014, and PhD from the Indian Institute of Science Education and Research Kolkata, India in 2021. She is now working as an Assistant Professor at the Department of Chemistry, Dhemaji College affiliated to Dibrugarh University, India. Her research interests include synthesis and application of π -conjugated systems, conjugated porous systems and optoelectronics.



Abhijeet R. Agrawal received his M.Sc. degree in Chemistry from S. G. B. Amravati University, India in 2013, and PhD from the Indian Institute of Science Education and Research Kolkata, India in 2021. He is now a postdoctoral fellow in the group of Prof. Ori Gidron at the Hebrew University of Jerusalem. His research interest includes developing easier synthesis methods for thiophene-containing conjugated systems, synthesis of twistacenes and crystal engineering.



Scheme 2. Different synthetic approaches to 2,4,6-tri(thiophen-2-yl)-1,3,5-triazine.

One of the earliest syntheses of 2,4,6-tri(thiophen-2-yl)-1,3,5-triazine or thienyltriazine was reported by Forsberg and co-workers in 1988 (Scheme 2) that involved lanthanide ion (Ln^{3+}) catalysed reaction between ammonia and 2-cyanothiophene (**2.1**). This led to the formation of mono-substituted amidine intermediate **2.2** which underwent further reaction with two molecules of **2.1** to afford the cyclized triazine derivative **2.3** in an overall 69% yield. The Ln^{3+} ions enhance the ion-dipole interaction assisted polarization of the cyano group thus promoting the addition of ammonia to it.^[45]

Another important synthesis of bithienyl-triazine derivatives (**2.7**, **2.8a/b/c**) was given by Chérioux and co-workers in 1998 (Scheme 2). It involved a triple aromatic nucleophilic substitu-

tion of 2,2'-dithienyllithium salts of **2.4** and **2.5** on cyanuric chloride. The mesomeric effect of the nitrogen atoms activates the substitution reaction and stabilizes the intermediate species, thus making this synthesis approach highly efficient. All the products could be easily isolated in more than 90% yield.^[46,47]

Thienyltriazine can also be prepared by employing the common metal-catalysed coupling reactions like the Stille coupling reaction, Suzuki coupling reaction, Kumada coupling reaction etc.^[48–54] Leriche and co-workers synthesized **2.3** by reaction between lithiated thiophene (**2.10**) or 2-tributylstannylthiophene (**2.9**) with cyanuric chloride (**2.6**) in 20% and 80% yields, respectively.^[55] Naka and co-workers made use of the

coupling approach given by Kumada and Tamao. This involved the Grignard cross-coupling reaction between thienylmagnesium bromide (**2.11**) and cyanuric chloride (**2.6**) to give **2.3** in 58% yield.^[56] Further **2.3** can also be obtained in an approximate 84% yield by Suzuki coupling reaction between 2-thienylboronic acid (**2.12**) and cyanuric chloride (**2.6**).^[57] The most straightforward, commonly adopted and easy synthesis of thienyltriazine (**2.3**) involves the cyclotrimerization reaction of 2-cyanothiophene (**2.1**) in presence of trifluoromethanesulfonic acid under cold conditions to afford the desired product in more than 70% yield.^[58–60]

Leriche and co-workers in their 2009 report also provided crystallographic insights into the structure of thienyltriazine, **2.3**. This compound crystallizes as two independent molecules in the orthorhombic $Pna2_1$ space group. The sum of the van der Waals radii for two sulfur atoms was 3.70 Å, whereas the S1...S4 contacts measured 3.512(2) Å and 3.534(2) Å which indicated the presence of intermolecular interactions (Figure 1, top). The sulfur atom and the carbon atom in 3-position of the thiophene ring are located at two positions, indicating the positional disorder effects in the molecule. The system is completely planar and the distance between two adjacent unit measures 3.40 Å or 3.46 Å. The triazine core from one molecule stacks with a little shift to the thiophene ring of the other molecule (Figure 1, bottom).^[55]

Cross-coupling reactions have become the most important synthetic tool for the preparation of novel class of organic compounds for applications in biology and material chemistry. These cross-coupling reactions necessitate the synthesis of different functionalized derivatives like the halides, stannyl, boronic acid or boronate, ethynyl etc.^[48–54] The preparation of different functionalized derivatives of thienyltriazine (**2.3**) is presented in Scheme 3. The synthesis of a triboronate derivative of **2.3**, i.e., **3.2**, was reported by Naka and co-workers.^[56] The first step involved the preparation of tribromo counterpart **3.1**, followed by the lithiation of **3.1** and finally reaction of the lithiated derivative with 2-isopropoxy-4,4,5,5-tetramethyl-1,3,2-dioxaborolane to afford the desired product in 72% yield. The bromination of thienyltriazine can be carried out under different conditions such as using Br_2 in CHCl_3 at around 60 °C or using *N*-bromosuccinimide (NBS) in CHCl_3 ^[60] or by using lithium diisopropylamide (LDA) in THF followed by the addition of $(\text{CF}_2\text{Br})_2$.^[61] The use of NBS for bromination of **2.3** is not a facile approach as it leads to a mixture of halide derivatives and their separation becomes cumbersome. The best approach for the preparation of the tribromo analogue **3.1** is by using Br_2 , as the electron-withdrawing nature of triazine makes aromatic electrophilic substitution at thiophenes difficult. However, for preparation of the dibromo derivative of thienyltriazine, i.e., **3.3**, using NBS in CHCl_3 is more appropriate.

The boronic acid derivative **3.4** can be obtained by treatment of the lithiated derivative of **2.3** (prepared by using freshly prepared LDA) with triisopropyl borate under negative temperature conditions followed by isolation of the product in 83% yield by treatment with acid.^[57] Under similar reaction conditions, replacing the borate derivative with tributyl tin chloride affords the tristannylated derivative **3.5** in more than 90%

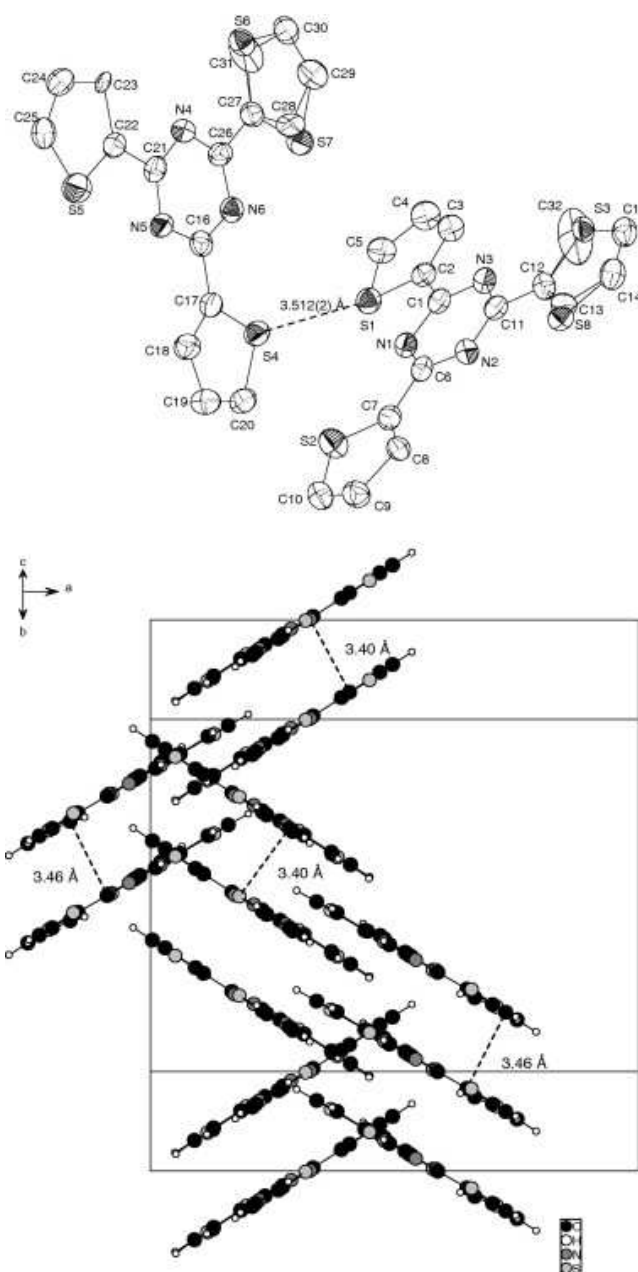
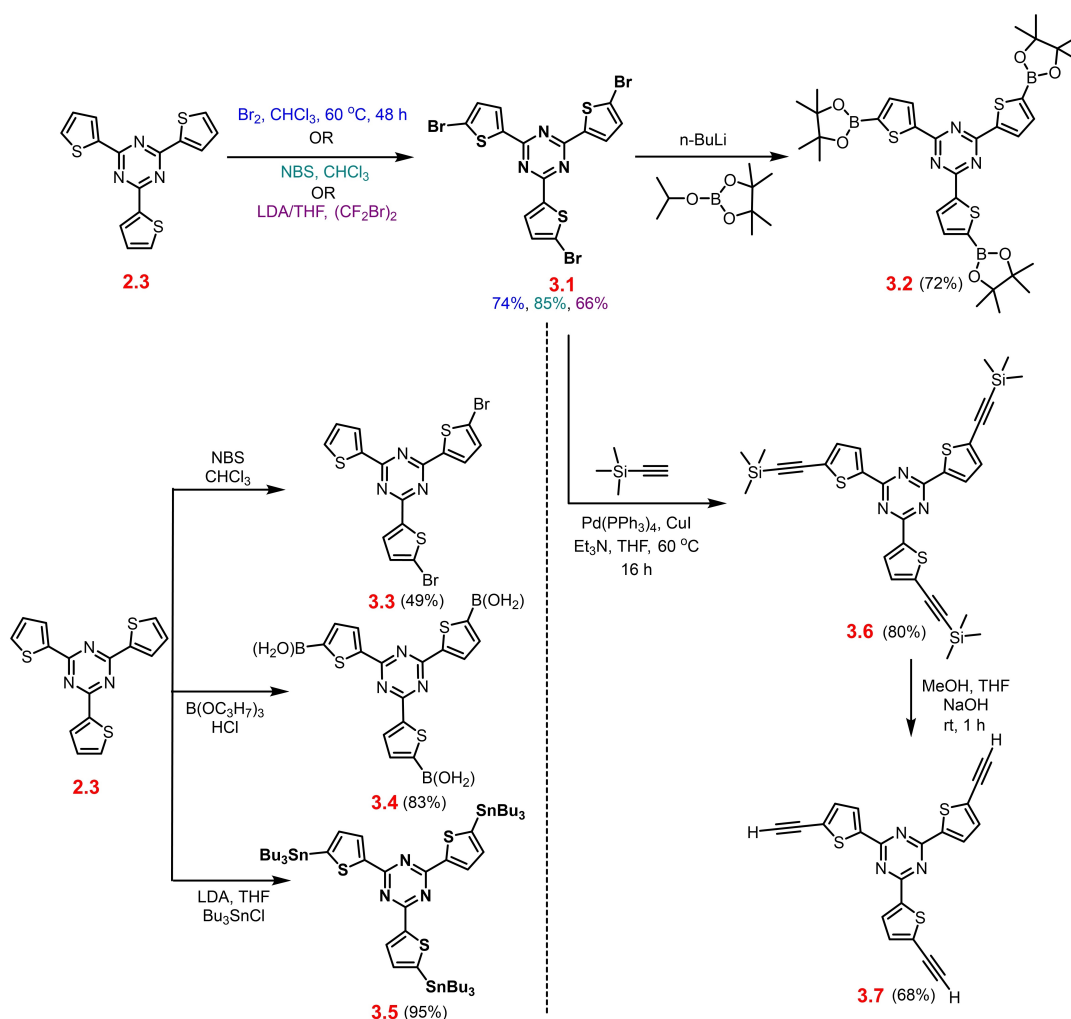


Figure 1. Top. Ortep view of derivative **2.3**, ellipsoids drawn at 50% probability level. Bottom. Part of the packing diagram in the unit cell. Reproduced with permission from Ref. [55], Copyright Elsevier, 2009.

yield.^[55] The triethynyl derivative of **2.3**, i.e., **3.7** can be obtained in approximately 68% yield by a Sonogashira coupling reaction of tribromo derivative **3.1** with trimethylsilyl acetylene followed by the deprotection of the silyl group under basic conditions.^[60]

All the derivatives mentioned above have been further used by researchers to prepare diverse class of materials. The use of thienyltriazine for the synthesis and application of different class of materials will be discussed below in coming sections in details.



Scheme 3. Synthesis of derivatives of 2,4,6-tri(thiophen-2-yl)-1,3,5-triazine.

3. Thienyltriazine-Based Systems and their Applications

The thiophene and triazine system present as the donor and acceptor unit, respectively, in thienyltriazine impart it with unique properties such as the push-pull effect, coplanarity, enhanced supramolecular, and π - π interactions. Besides that, the molecule possesses a C_{3h} symmetry which makes it an ideal candidate for application in material chemistry. This has led to wide application of the thienyltriazine system for the synthesis of star type molecules, linear and hyperbranched polymers, wide class of porous materials etc. Detailed insights into each of the class is discussed in the coming sections.

3.1 Thienyltriazine-based star molecules

Star-shaped molecules are class of branched compounds in which more than two arms are attached in a symmetrical fashion to a single multifunctional core. The first star-shaped polyamides were reported in 1948 by Flory and co-workers and

later on, in 1962, Morton and co-workers reported star-shaped branched polystyrenes polymer prepared through anionic polymerization.^[62,63] It was after this report that branched systems with three or more arms were referred as star systems. Star-based systems have become promising materials in different fields like optoelectronics, electrochromic devices, biological applications, liquid crystalline materials etc. The defined molecular weight, defined molecular structure, easy purification, reproducibility in devices etc. are some of the factors that make star molecules superior to the polymer materials.^[64-67] Symmetric systems like triphenylamine, 2,4,6-trisubstituted 1,3,5-triazine, 1,3,5-trisubstituted benzene etc. have been some of the most interesting precursors for the synthesis of star molecules.^[68] Thienyltriazine has become an attractive candidate for the synthesis of star-shaped small molecules that find diverse applications besides being used to establish structure-property relationship. These examples are discussed below in detail.

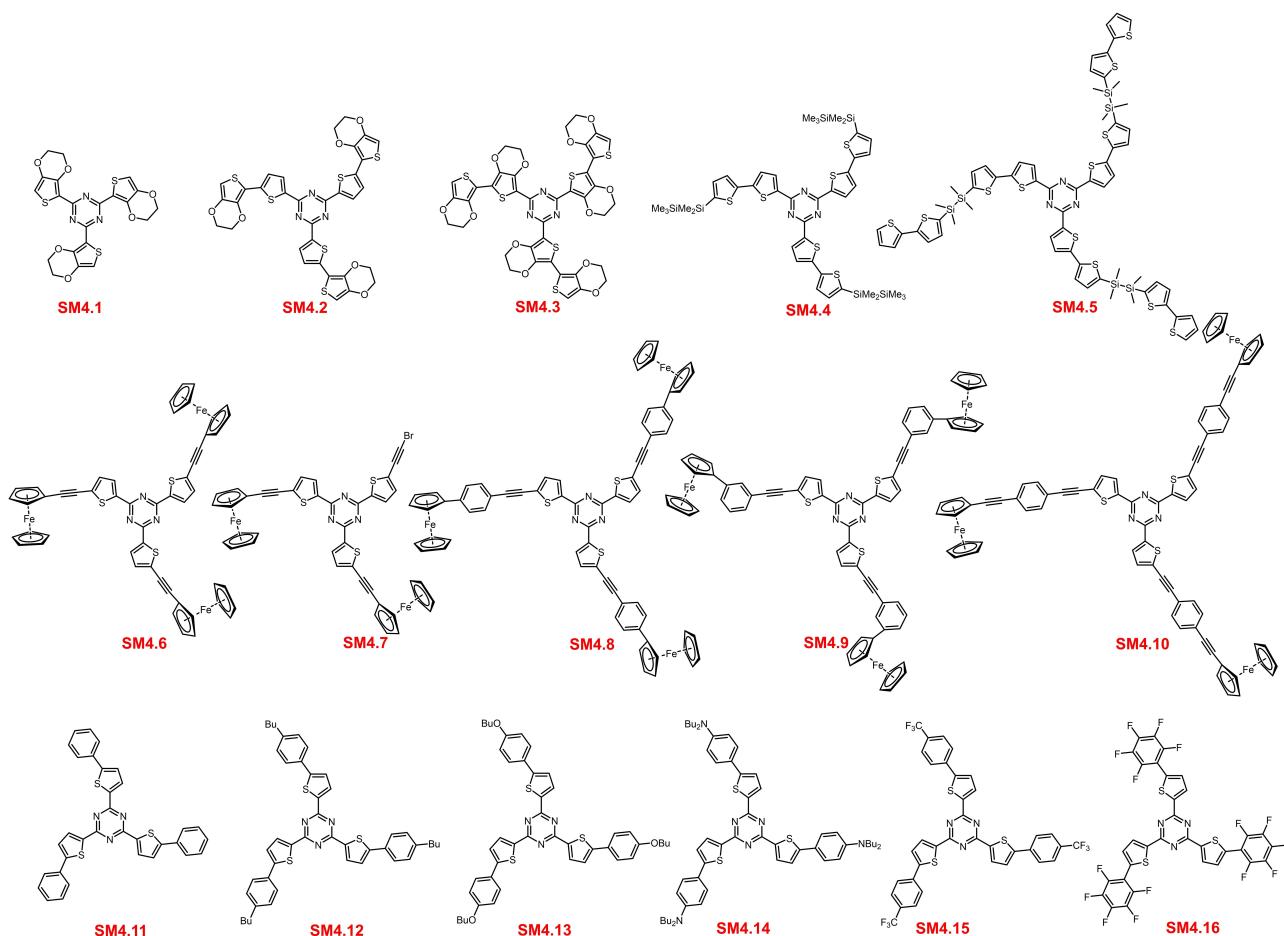
3.1.1 Structure-property relationships

The first report of thienyltriazine-containing star molecule polymers was given by Chérioux and co-workers. These compounds were the bithienyl-substituted triazine derivatives **2.7** and **2.8a**, and their synthesis has been discussed in Scheme 2. Electrochemical insights revealed that the voltammograms were irreversible for **2.7** irrespective of the scan rate up to 1000 V s^{-1} , indicating a very high reactivity of the electro-generated cation radical species. Molecule **2.8a** showed an oxidation potential of 1.27 V vs. SCE (saturated calomel electrode) at 1 V s^{-1} with a return peak. In this case, the propylthio group blocks the α positions and hence the cation radicals can neither undergo coupling nor nucleophilic attack due to the sterics arising from the triazine centre. The oxidation of an adsorbed species was always observed in the return peak irrespective of the solvent indicating the less solubility of the electrogenerated cation radical.^[46]

Based on their previous report, Chérioux and co-workers further prepared butyl-substituted and allyl-substituted analogues of **2.8a**, that is **2.8b** and **2.8c**, in almost 90% yield, respectively (Scheme 2). The butyl chain was introduced to enhance the solubility of the final molecule and the allyl chain was introduced with the aim to polymerize the allyl precursor.

Insights into the electronic properties of these octupoles revealed a complete planar arrangement with D_{3h} symmetry and an absorption band centred at 380 nm . These octupoles also showed off-resonant third order non-linear optical (NLO) properties and a relative nonlinear index of 0.6. In accordance with the position of the linear absorption peak wavelengths, a two-photon absorption band was observed around 760 nm quite far from the exciting wavelength.^[47]

Leriche and co-workers established structure-property relationships of short-chain oligothiophenes attached to the triazine core. These donor-acceptor systems include **2.3**, **SM4.1**, **2.7**, **SM4.2** and **SM4.3** (Scheme 2 and Scheme 4) and were synthesized by utilising a Stille coupling strategy in 80%, 90%, 60%, 83%, and 30% yield, respectively. As expected, an increase in the number of 3,4-ethylenedioxythiophene (EDOT) units present in the branch led to an increase in the wavelength of absorption and consequently a decrease in the oxidation potential. **SM4.3** had two EDOT units on each arm and hence its two successive oxidation waves were observed at 0.80 V and 1.10 V compared to 0.98 V and 1.17 V for **SM4.2**. **SM4.1**, **SM4.2** and **SM4.3** could also be electrochemically polymerized into the corresponding electroactive polymers with decreased oxidation potential compared to the polymers.^[55]



Scheme 4. 2,4,6-Tri(thiophen-2-yl)-1,3,5-triazine-based star molecules used to establish structure-property relationships.

Star-like systems **SM4.4** and **SM4.5** (Scheme 4) consisting of the electron-accepting triazine core and electron-rich bithienylene arms with an alternative arrangement of Si–Si bonds were reported by Naka and co-workers.^[56] **SM4.4** and **SM4.5** were prepared by the Pd-catalysed reactions of 2,4,6-tris[5-(1,3-dioxo-4,4,5,5-tetramethyl-2-borolanyl)-2-thienyl] triazine with 5-bromothierylpentamethyldisilane and 1-(5-bromothieryl)-2-bithienyltetramethyldisilane, respectively in 30% and 23% yield, respectively. Mizuno and co-workers in their report discussed that introduction of silyl substituents enhanced the fluorescence intensities of the resulting systems.^[69] As envisioned, photophysical insights revealed higher fluorescence quantum yields of 0.67 and 0.96 for **SM4.4** and **SM4.5**, respectively, which was significantly higher than the same for 2,4,6-tris(bithienyl)triazine (Figure 2A).

Donor- π -acceptor type symmetrical triazine containing star molecules **SM4.6**, **SM4.7**, **SM4.8**, **SM4.9** and **SM4.10** were synthesized with an aim to establish the influence of ferrocene and varying spacer units on the electronic properties of the resulting systems. **SM (4.6-4.10)** were obtained by Pd-catalysed Sonogashira coupling reaction in 52%, 57%, 39%, 40% and 32% yields, respectively (Scheme 4). All the star molecules (SMs) showed strong absorption centred between 349 nm and 382 nm arising from π - π^* transitions and confirm the presence of intramolecular charge transfer from ferrocene core to the triazine core (Figure 2B). The charge transfer bands of **SM4.8**, **SM4.9** and **SM4.10** overlapped with the π - π^* transition band and hence could not be observed separately. The following trend observed in the oxidation potential **SM4.6** > **SM4.10** > **SM4.8** > **SM4.9** is indicative of the nature of the spacer group. For example, **SM4.9** containing a *meta*-branched spacer disrupts the π -conjugation and hence exhibits lower oxidation potential compared to **SM4.6**, **SM4.8** and **SM4.10**. Similarly, **SM4.6** with an acetylenic spacer features extended π -conjugation and hence has higher oxidation potential compared to other **SM4.8**, **SM4.9** and **SM4.10** and is indicative of efficient electronic communication between the donor and acceptor counterparts. Besides being non-emissive, all the SMs exhibited good thermal stability with the following order **SM4.10** >

SM4.6 > **SM4.8** > **SM4.9** and this was indicative of the robustness of **SM4.10** and **SM4.6**.^[60]

The effects of electronic nature of the terminal aryl groups on the thienyltriazine systems were studied by Muraoka and co-workers where they synthesized star-type molecules **SM4.11**–**SM4.16** (Scheme 4) by using Suzuki coupling reactions in yields ranging from 28–90%.^[61] These SMs had tuneable photophysical properties. SMs with the most electron-rich donor (dibutylamino group), i.e., **SM4.14** exhibited absorption and emission solvatochromic properties due to efficient intramolecular charge transfer. The absorption maximum of **SM4.15** was greater than that of **SM4.16** guided by the electron-donating strength of the aryl group pentafluorophenyl > *p*-trifluoromethylphenyl and the other compounds also showed a trend **SM4.14** > **SM4.13** > **SM4.12** > **SM4.11** guided by the electron donating strength of the aryl counterpart which is *N,N*-dibutylaminophenyl > *p*-butoxyphenyl > *p*-butylphenyl > phenyl. Electrochemical insights revealed that the HOMO energy level increases in the order **SM4.14** > **SM4.13** > **SM4.12** > **SM4.11** > **SM4.15** and the LUMO level increases in the order of **SM4.15** < **SM4.11** < **SM4.12** < **SM4.13** < **SM4.14** and the trend are in accordance with the electron donation ability of the aryl substituents. **SM4.14** with a reversible oxidation wave at +0.51 V showed an overall three-electron transfer process due to formation of tri-radical cation species containing three amino radical cation segments. Besides that, **SM4.14** exhibited colorimetric and luminescence proton sensing properties as witnessed by a change in the UV-Vis absorption spectra by addition of increasing amounts of trifluoroacetic acid (TFA; Figure 3A). The terminal amino group and the nitrogen atoms on the triazine core act as proton-sensitive receptors.

In a separate report in 2016, Zhong and group reported an electrochromic device using thienyltriazine **2.3** as an electrochromic active layer and the device structure involved **2.3**/conducting gel/ITO (Indium tin oxide). Electrochemical doping and de-doping of **2.3** as a solid film in between potential +1.9 V and –1.9 V resulted in a colour change from colourless to orange-yellow as shown in Figure 3B. This report indicated

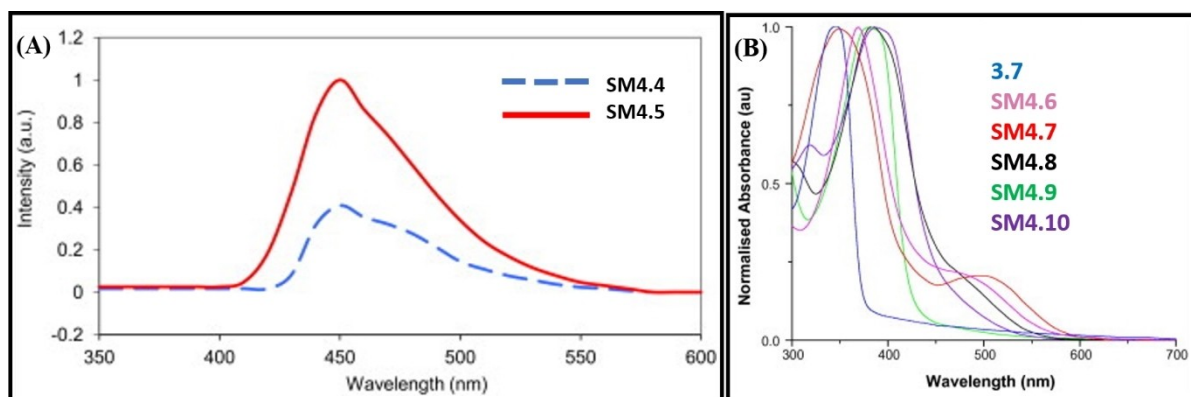


Figure 2. (A) Fluorescence spectra of **SM4.4** and **SM4.5** in 10^{-5} M dioxane solution. Reproduced with permission from Ref. [56]. Copyright Elsevier, 2012. (B) Normalised electronic absorption spectra of triazines **3.7**, **SM4.6**–**SM4.10** in CH_2Cl_2 (1×10^{-4} M solution). Reproduced with permission from Ref. [60]. Copyright Elsevier, 2013.

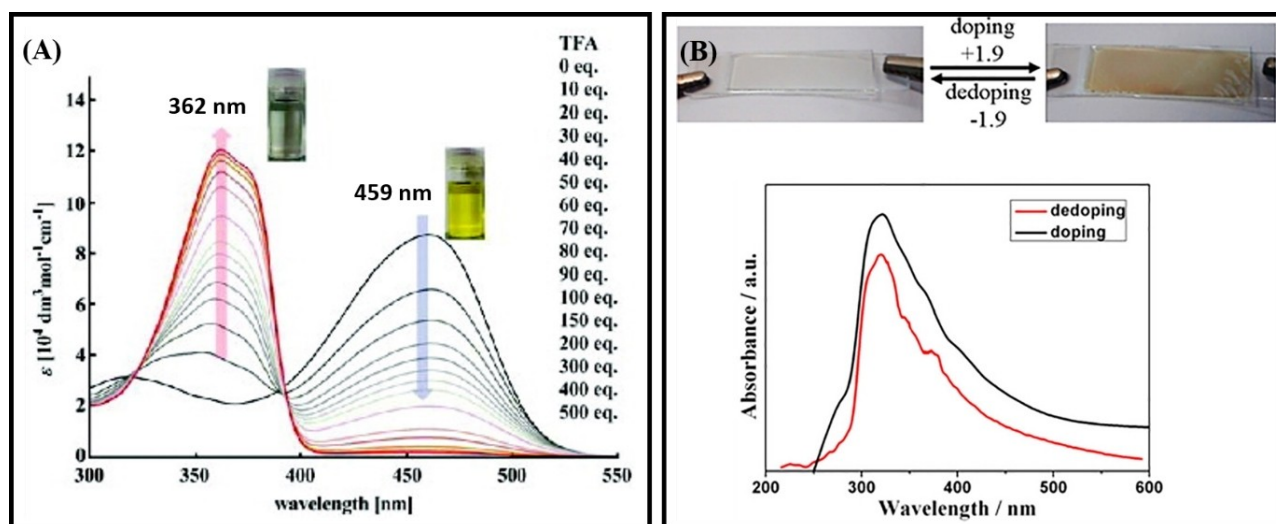


Figure 3. (A) Change in the UV-Vis absorption spectra of compound **SM4.14** in CH_2Cl_2 solution ($10 \mu\text{mol dm}^{-3}$) at ambient temperature with addition of TFA (0–500 eq.). Reproduced with permission from Ref. [61]. Copyright Taylor and Francis, 2015. (B) Electrochromic photographs and the electronic absorption spectra of a 2,4,6-tri(thiophen-2-yl)-1,3,5-triazine (**2.3**) solid film on electrochemical doping and de-doping. Reproduced with permission from Ref. [70]. Copyright Taylor and Francis, 2015.

the potential of thienyltriazine as a promising electrochromic material.^[70]

3.1.2 Materials with two-photon absorption behaviour

Two-photon absorption is a third-order nonlinear optical property that involves absorption of two low-energy photons at the same time leading to a high-energy excited state. The two-photon absorption phenomenon finds its application in several fields like photodynamic therapy,^[71] optical power limiting,^[72] two-photon fluorescence excitation microscopy,^[73] 3D optical data storage,^[74] two-photon upconversion lasing^[75] etc. The triazine core, offering a strong electron-accepting ability and coplanarity when connected with aryl substituents, has been widely explored for the synthesis of materials with large two-photon absorption cross-section.^[76–78]

Zou and co-workers synthesized star-shaped molecules **SM5.1–SM5.7** (Scheme 5) in yields exceeding 65% by using palladium-catalysed cross-coupling reactions.^[79] **SM5.5**, **SM5.6** and **SM5.7** had the same core, thienyltriazine, and same arms (triphenylamine, carbazole and fluorene, respectively) as **SM5.1**, **SM5.2** and **SM5.3**, respectively with the difference that the former had an acetylene spacer between the core and arms. Photophysical insights revealed that changing the end group can significantly influence the optical properties. The electron-donating strengths of the arms follow the order triphenylamine > 3-(*N*-alkylcarbazole) > 2-(*N*-alkylcarbazole) \approx 2-(9,9-dialkylfluorene) and hence, the order of UV-Vis absorption maxima is **SM5.1** > **SM5.2** > **SM5.3** > **SM5.4**. The same trend was also observed for **SM5.6–SM5.7**. The UV-Vis absorption maximum is influenced by both the strong intramolecular charge transfer

(ICT) effect and π -conjugation efficiency. Electrochemical insights reveal that all compounds exhibit reversible or quasireversible redox behaviour and the band gap of the star molecules decreases as the electron-donating strength of the end group increases. All the SMs exhibited two-photon absorption in the wavelength range 720–880 nm with large two-photon absorption cross-section area associated with strong intramolecular charge transfer (Figure 4). The maximum of the two-photon cross-section ($\sigma_{2\text{max}}$) increases with the increase in the electron-donating strength of the end group.

In continuation of their 2013 report,^[60] Maragani and co-workers studied the linear and nonlinear optical properties of the star-shaped ferrocenyl substituted thienyltriazines **SM4.6**, **SM4.8**, **SM4.9** and **SM4.10** (Scheme 4). Photophysical and electrochemical insights revealed that the red shift in the π - π^*

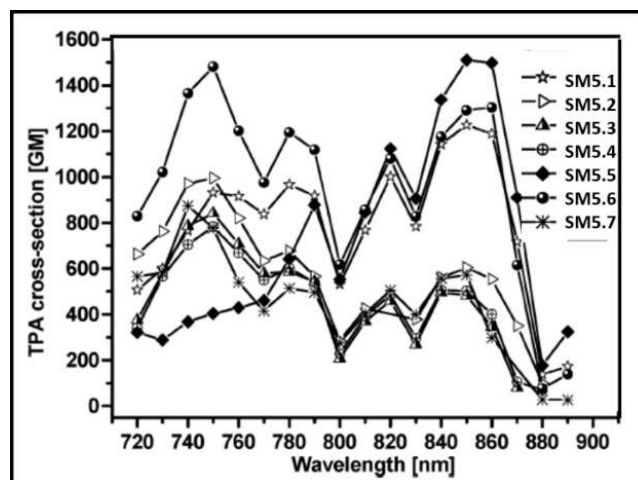
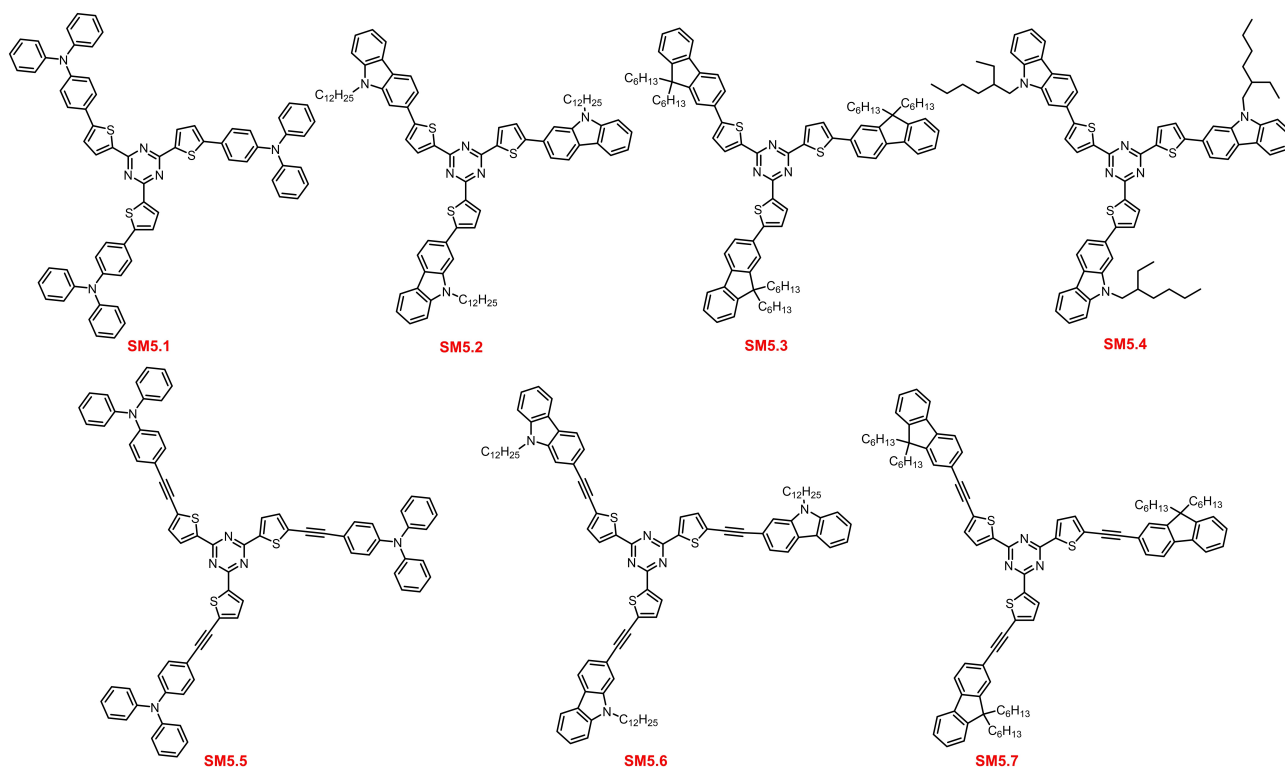


Figure 4. Two-photon absorption spectra of **SM5.1–SM5.7**. Reproduced with permission from Ref. [79]. Copyright John Wiley and Sons, 2009.



Scheme 5. 2,4,6-Tri(thiophen-2-yl)-1,3,5-triazine-based star molecules displaying two-photon absorption behaviour.

absorption and enhancement in molar extinction coefficient in **SM4.6**, **SM4.8–SM4.10** were directly proportional to the conjugation length whereas the HOMO–LUMO gap was inversely proportional to the conjugation length. The most conjugated ferrocenyl triazine system **SM4.10** exhibited a large two-photon absorption coefficient value of around 1.8×10^{-13} m²/W.^[80]

3.1.3 Materials with liquid crystalline behaviour

The controlled self-assembly of conjugated entities based on supramolecular interactions can help in tailoring their properties, and introduction of liquid crystallinity in π -conjugated materials is one of the convenient ways to control molecular

self-organization.^[81–84] Due to different types of non-covalent interactions arising individually due to thiophene and triazine systems, the thienyltriazine system has been explored in the field of liquid crystalline materials.^[85]

Yasuda and co-workers in their work synthesized conductive columnar materials **SM6.1(a–c)**, **SM6.2**, and **SM6.3** by palladium-catalysed coupling reaction in yields between 80–90%. (Scheme 6).^[86] Time-of-flight measurements revealed that these octupoles can self-organize into 1D columnar nanostructures as shown in Figure 5A. Polarizing optical photomicrographs of **SM6.1 b** in the Col_h phase at 100 °C are shown in Figure 5B. Electrochemical insights revealed that all octupoles can undergo both electrochemical oxidation and reduction because of the inherent D–A nature and the E_{LUMO} values of the

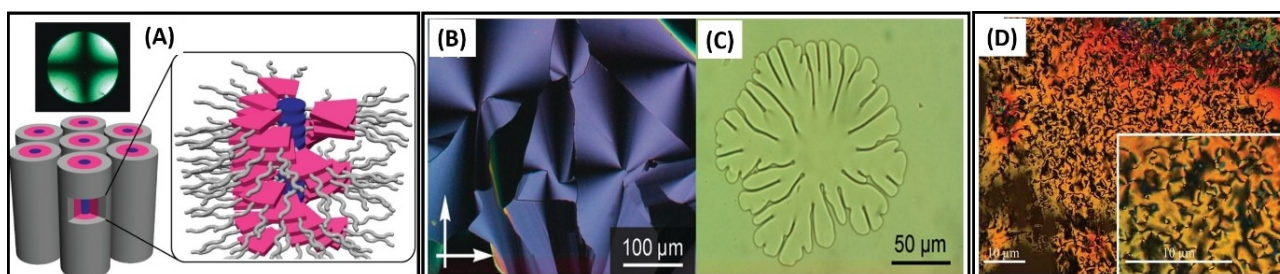
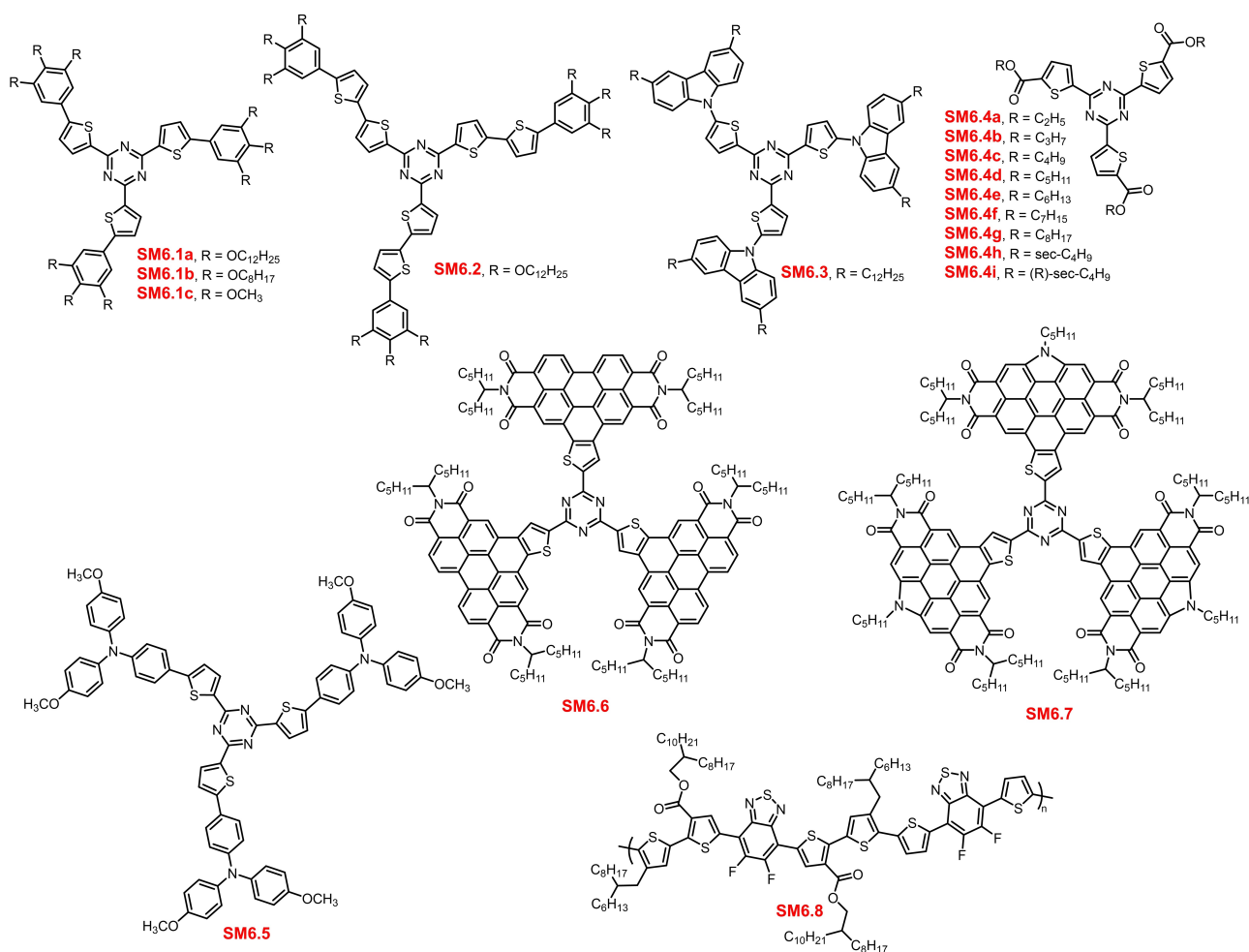


Figure 5. (A) Schematic illustration of the homeotropically aligned Col_h structure of **SM6.1 a**. The blue, pink and grey portions stand for the triazine cores, phenylthiophene units, and alkyl chains, respectively. (B) Polarizing optical photomicrograph of **SM6.1 b** in the Col_h phase at 100 °C. (C) Dendritic growth of a homeotropic domain of **SM6.1 b** on slow cooling (1 °C min⁻¹) with uncrossed polarizers. The arrows indicate the directions of polarizer and analyser axes. Reproduced with permission from Ref. [86]. Copyright American Chemical Society, 2011. (D) Schlieren textures of **SM6.4 e** at two different magnifications (crossed polarizers, 45 °C). Reproduced with permission from Ref. [88]. Copyright Taylor and Francis, 2018.



Scheme 6. 2,4,6-Tri(thiophen-2-yl)-1,3,5-triazine based star molecules showing liquid crystalline behaviour (**SM6.1**, **SM6.2**, **SM6.3** and **SM6.4**) and those used as photovoltaic materials (**SM6.5**, **SM6.6**, **SM6.7** and **SM6.8**).

compounds, i.e., -3.0 eV, were comparable to that of widely used electron-transporting material Alq₃.^[87] The charge carrier mobility studies revealed that **SM6.1a** exhibited hole and electron mobilities as $\mu^+ = 3 \times 10^{-5}$ and $\mu^- = 4 \times 10^{-3}$ cm²V⁻¹s⁻¹ at 100 °C, respectively, whereas **SM6.1b** exhibited the same on the order of 10^{-5} and 10^{-3} cm²V⁻¹s⁻¹ respectively, in the Col_h phase. The 100 times faster electron mobilities in both cases was attributed to the octupolar structure of the propeller-shaped SM and the trigonally ramified phenylthiophene arms. The triazine core enhances the stacking between the molecules, thus leading to highly efficient 1D electron transport. **SM6.2** and **SM6.3** did not show any electron mobilities but exhibited highly enhanced hole mobilities of the order 10^{-2} cm²V⁻¹s⁻¹ attributed to increased intermolecular π - π interaction arising due to electron-rich segments.

Taing and co-workers reported the synthesis of SMs involving *s*-triazine cores substituted with three thiophene carboxylate groups (Scheme 6).^[88] Nine derivatives with linear, branched, and chiral ester chains were synthesized [**SM6.4(a-i)**] with yields ranging between 14–93%. Their mesomorphism was studied by polarised optical microscopy, differential scanning calorimetry, and powder X-ray diffraction. Triazines

with linear propyl to octyl chains **SM6.4b**-**SM6.4g** displayed monotropic nematic discotic mesophases that crystallised within hours or days or when mechanically agitated. Packing structures for the nematic phases were proposed based on the single crystal structure of the ethyl ester. **SM6.4e**, **SM6.4f**, **SM6.4h** and **SM6.4i** had unusually slow nucleation and crystal growth, probably due to the large number of possible low-energy conformations that arise from the conformationally flexible core. The nucleation and crystal growth could be enhanced by incorporation of racemic and chiral branched chains as was the case observed for **SM6.4h** and **SM6.4i** with lowered melting points. Chiral nematic discotic mesophases were obtained for binary mixtures of derivatives with chiral branched and linear chains **SM6.4e** and **SM6.4i** (Figure 5D).

3.1.4 Materials for photovoltaic applications

Combining donor-acceptor systems with conjugated systems is a well-known strategy for designing low energy gap/band gap materials. Thienyltriazine-based star molecules have shown remarkable results in this direction. **SM6.5** was synthesized by

using the Stille coupling reaction of 2,4,6-trichloro-1,3,5-triazine with *N,N*-bis(4-methoxyphenyl)-*N*-[(5-(tributylstannyl)thiophen-2-yl)phenyl]amine in ~50% yield (Scheme 6). The UV-Vis absorption study revealed the absorption maximum of **SM6.5** to be at 429 nm and its emission maximum was observed to be at 502 nm with a small Stokes shift of 73 nm. **SM6.5**, being used as a hole-transporting material in perovskite solar cells, exhibited a remarkable power conversion efficiency (PCE) of 12.51% with a J_{sc} of 20.74 mA cm⁻², a V_{oc} of 0.92, and a fill factor (FF) of 66%. Moreover, a **SM6.5**-based cell showed a good stability for 250 h.^[89]

In 2021, Deng and co-workers designed the synthesis of thienyltriazine and perylene diimide-containing propeller-like star molecules **SM6.6** and **SM6.7** (Scheme 6).^[90] The thiophene units of thienyltriazine prevented the overcrowding of the triazine cores by the perylene diimide (PDI) arms and also the sulfur atom of thiophenes led to N...S non-covalent interactions that provided the propeller-shaped molecules with a conformational lock. The smaller triazine core also reduced the distance between the PDI arms and enhanced the intramolecular charge transport. In **SM6.7**, an *N*-annulation strategy was used on the outer bay position of each PDI arm. The arylamine chain in **SM6.7** reduced its crystallization tendency due to steric factors. Both molecules displayed excellent thermal stability and photophysical studies revealed a strong absorption from 450–550 nm in solution. The optical band gaps were calculated to be 2.13 eV for both the molecules whereas the electrochemical band gap were found to be 2.32 eV and 2.40 eV for **SM6.6** and **SM6.7**, respectively. The slightly lower band gap of **SM6.7** was attributed to its low crystallization tendency which reduces intermolecular aggregation. These molecules were explored in photovoltaic devices with **SM6.8** as the donor polymer. For **SM6.8:SM6.6**, a top PCE of 8.75% was obtained with V_{oc} of 1.06 V, J_{sc} of 12.19 mA cm⁻², and FF of 67.78%. The **SM6.7**-based devices showed improved performances with top PCE reaching 10.52%, V_{oc} of 1.12 V, J_{sc} of 13.09 mA cm⁻² and FF of 71.76%. However, **SM6.7** showed significantly lower electron mobilities due to the hindered intermolecular aggregation arising due to the extra side chain.

3.1.5 Other miscellaneous applications

Besides the above discussed applications, thienyltriazine containing systems have also been used as flame retardant materials, sensing materials etc.

Zhang and co-workers, in two separate reports, explored the synergistic effect of boronic acid derivative of thienyltriazine (**3.4**) on the flame retardancy of epoxy resin and the results showed that boronic acid derivative alone or along with Mg(OH)₂ can inhibit combustion effectively without decreasing the mechanical strength.^[91,92]

Thienyltriazine cores with 1-aza 15-crown 5-ether and dipicolylamino groups as receptors arms were used to synthesize star-shaped (D-π)₃-A molecules **SM7.1** and **SM7.2** (Scheme 7) in 71% and 60% yields, respectively, by using the Suzuki-Miyaura coupling reaction. Photophysical insights revealed the absorption maxima for the two compounds to be located at 450 nm and 435 nm, respectively, whereas their emission maxima were located at 553 nm and 547 nm, respectively. Besides that, both molecules exhibited strong ICT and ICT-based optical properties. Both **SM7.1** and **SM7.2** exhibited spectral blue shifts followed by red shifts upon protonation. **SM7.1** also exhibited a similar shift upon stepwise complexation of Mg²⁺ (Figure 6A), whereas **SM7.2** exhibited a blue shift upon complexation with Zn²⁺ (Figure 6B). The initial blue shift occurs due to the decreased ICT donor capacity of the amino-donor-type receptors on binding with cations and the second red shift was attributed to the enhanced acceptor ability of the triazine core upon binding cations.^[93] Such systems can be used for visual and distinct detection of both protons and metals ions.

Park and co-workers reported new trinuclear complexes of Pd²⁺ and Pt²⁺, **SM7.3** and **SM7.4** (Scheme 7), containing C_{3h}-symmetric thienyltriazine obtained by triple oxidative addition reactions. A Sonogashira-type coupling of trinuclear Pt²⁺ halide complex, i.e., **SM7.4** with alkynes, in the presence of cuprous halide and diethylamine, formed the corresponding alkynyl Pt²⁺ complex **SM7.5**.^[94]

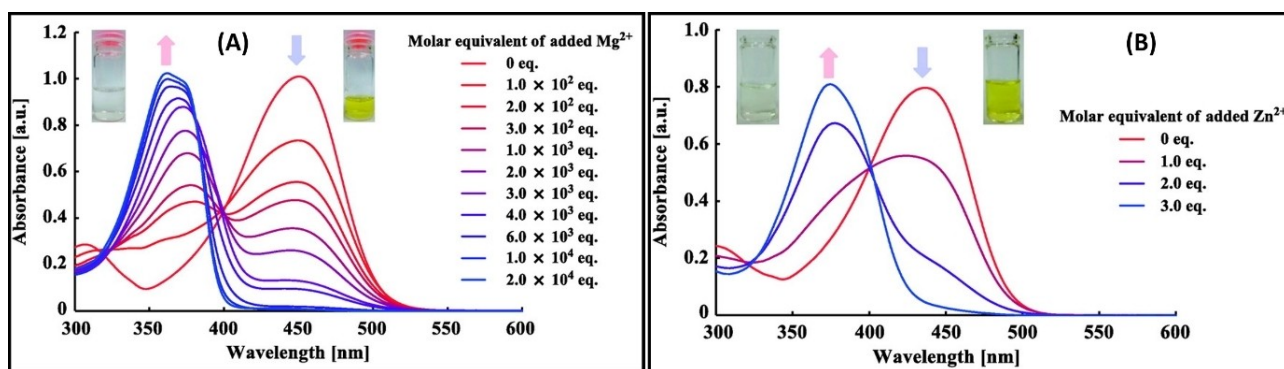
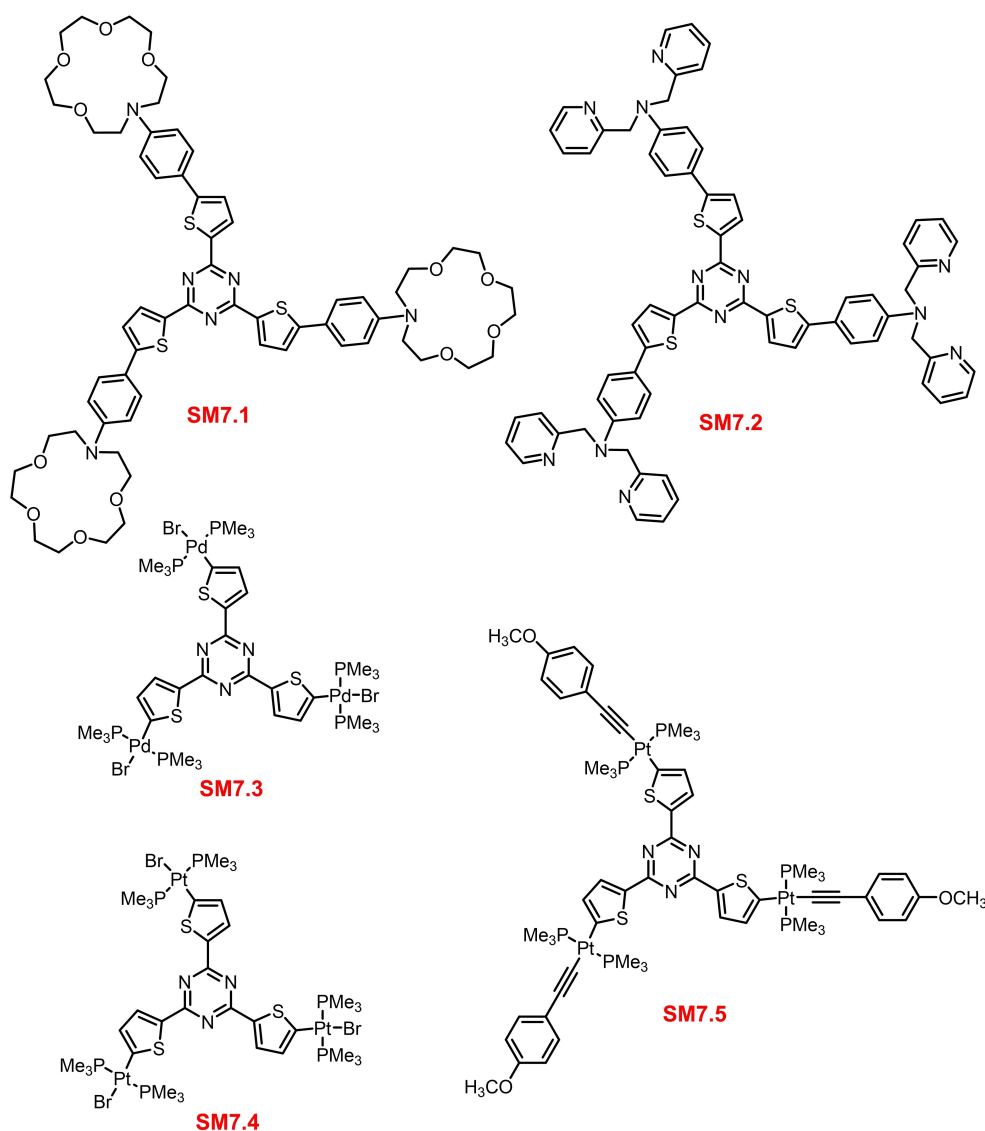


Figure 6. (A) First-step changes in the UV-Vis absorption spectrum of **SM7.1** (10 μmol dm⁻³) CH₂Cl₂-CH₃CN solution (1:1, v/v) upon the gradual addition of Mg²⁺ (0 to 2.0 × 10⁴ eq.). (B) Changes in the UV-Vis absorption spectrum of **SM7.2** (10 μmol dm⁻³) CH₂Cl₂-CH₃CN solution (1:1, v/v) upon the gradual addition of Zn²⁺ (0 to 3.0 eq.). Reproduced with permission from Ref. [93]. Copyright Chemical Society of Japan, 2019.



Scheme 7. 2,4,6-Tri(thiophen-2-yl)-1,3,5-triazine-based star molecules for sensing (PM7.1 and PM7.2) and catalytic applications (PM7.3 and PM7.4).

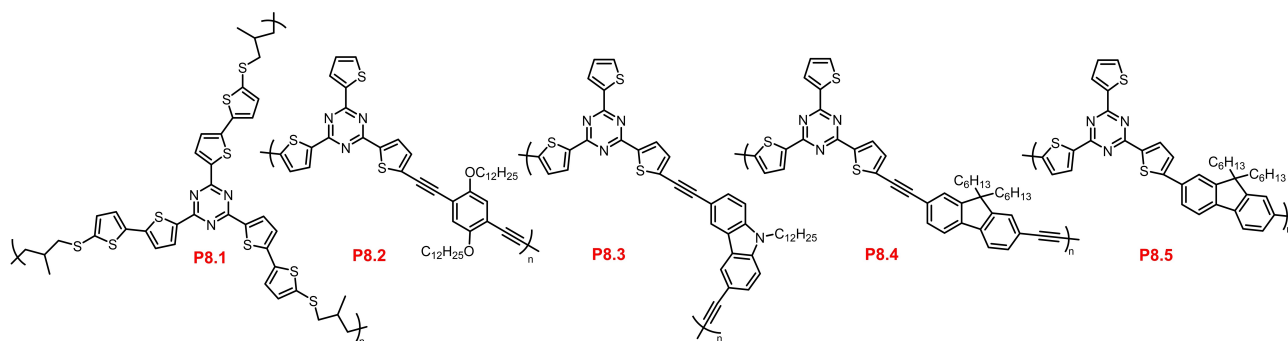
3.2 Thienyltriazine-based linear and hyperbranched polymers

Linear thienyltriazine polymers are prepared by using its difunctionalised derivative whereas hyperbranched polymers are prepared by using its trifunctionalized derivative.

The first example of thienyltriazine containing octupolar polymer, **P8.1** was given by Chérioux and co-workers in 1999 (Scheme 8). The polymer was synthesized by radical homopolymerization of octupolar monomer **2.8c** with azobisisobutyronitrile (AIBN) as radical initiator. The UV-Vis absorption spectrum of the polymer revealed a narrow linear absorption band centred at 376 nm. The polymer was also explored for its off-resonant third order nonlinear optical properties.^[47]

Zou and co-workers designed and synthesized π -conjugated thienyltriazine-based linear polymers **P8.2**, **P8.3**, **P8.4** and **P8.5** (Scheme 8). **P8.2**, **P8.3** and **P8.4** involved a Sonogashira coupling reaction between the dibromo thienyltriazine counter-

part and 2,5-bis-dodecyloxy-1,4-diethynyl-benzene, 3,6-diethynyl-9-dodecyl-9H-carbazole and 2,7-diethynyl-9,9-dihexyl-9H-fluorene, respectively, to give the polymers in yields greater than 60%. **P8.5** was synthesized by a Suzuki coupling reaction between dibromo thienyltriazine and 9,9-di-*n*-hexylfluorene-2,7-bis(trimethylboronate). All the polymers displayed excellent thermal stability and the decomposition temperature was highest for **P8.5** (~429 °C). Polymer **P8.3** had a rigid structure due to presence of single alkyl chain and hence it lacked any glass transition temperature. Photophysical insights revealed that the thin film UV-Vis absorption maximum of the polymers followed the trend **P8.2** > **P8.5** > **P8.4** > **P8.3** and the emission maximum followed the trend **P8.3** > **P8.2** > **P8.5** > **P8.4** (Figure 7A). The observed trend of quantum yields of the polymers was **P8.5** > **P8.4** > **P8.3** > **P8.2**. The UV-Vis absorption was observed in two regions viz. 420–490 nm and 300–350 nm, the former arising due to π - π^* electron transition due to donor-acceptor attributed extended conjugation and the latter arising



Scheme 8. 2,4,6-Tri(thiophen-2-yl)-1,3,5-triazine based linear polymers.

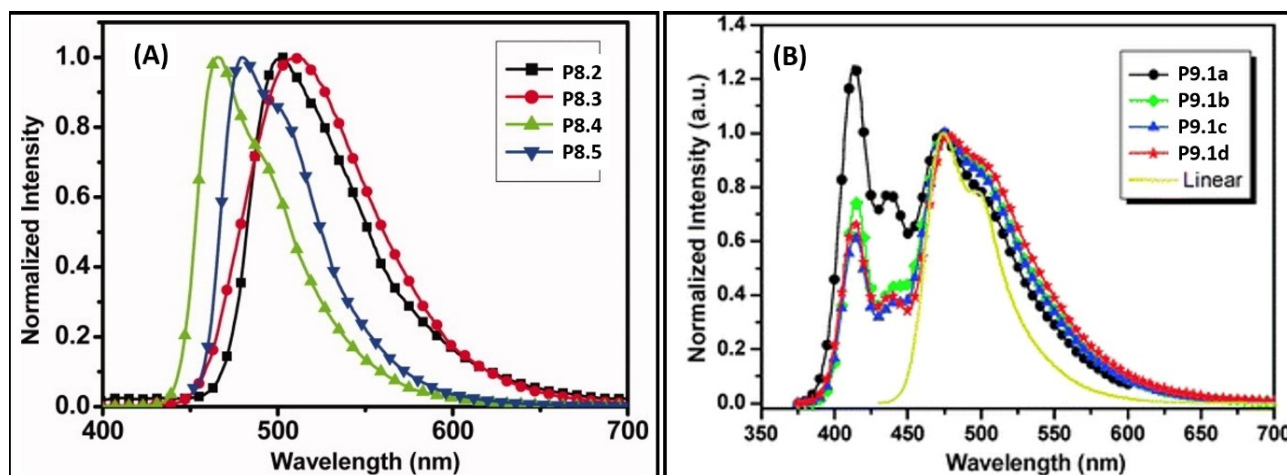
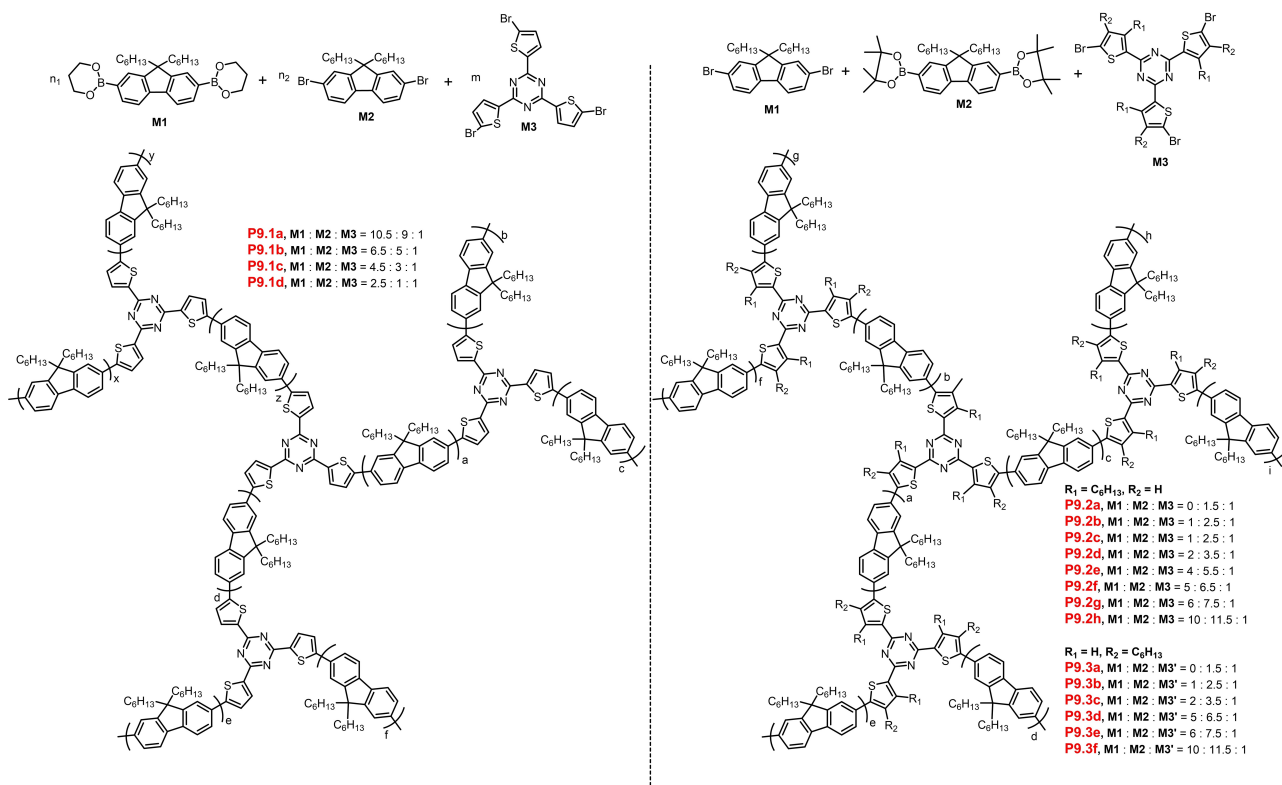


Figure 7. (A) Photoluminescence spectra of the polymers **P8.2**, **P8.3**, **P8.4** and **P8.5** in solution. Reproduced with permission from Ref. [95]. Copyright John Wiley and Sons, 2007. (B) The fluorescence emission spectra of **P9.1 a/b/c/d** and the linear polymer in THF measured upon excitation at 360 nm. Reproduced with permission from Ref. [97]. Copyright Royal Society of Chemistry, 2011.

from the localised π -conjugated system. The low quantum yields of polymers **P8.2** and **P8.3** in solution was due to two factors, first is the increased donor strength and second is the coplanarity-assisted molecular aggregation that weakens the fluorescence efficiency. The low quantum yield of **P8.4** was attributed to the hindered molecular aggregation due to the two long alkyl chains and the red-shifted emission maximum and high quantum yield of **P8.5** was due to the efficient conjugation and absence of an alkyne spacer. The presence of the triazine core imparts all the polymers with low lying LUMO (-2.86 to -3.06 eV) thus making them ideal candidates for electron transport.^[95]

The two-photon absorption property of polymers **P8.2**, **P8.4**, and **P8.5** was studied by Mariz and co-workers. An increase in the electron-donating strength of the donor caused an increase in the mass-weighted two-photon absorption cross-section. The conjugation length of the polymer was directly proportional to the two-photon absorption cross-section and hence the same was greater for **P8.4** as compared to **P8.5**. These polymers were also used to prepare water-soluble polymer dots of diameter 60–70 nm and with a two-photon absorption (TPA) cross-section of the order of 10^6 GM.^[96]

Thienyltriazine-containing hyperbranched polymers synthesized by using monomers in different ratios were reported by Zou and co-workers. These polymers with 2,4,6-tri(thiophen-2-yl)-1,3,5-triazine cores and polyfluorene chain arms were synthesized using Suzuki coupling reactions with a $A_2 + A_2' + B_3''$ methodology and ratios of the monomers as **P9.1 a**, M1:M2:M3 = 10.5:9:1; **P9.1 b**, M1: M2: M3 = 6.5:5:1; **P9.1 c**, M1:M2:M3 = 4.5:3:1 and **P9.1d**, M1:M2:M3 = 2.5:1:1, respectively (Scheme 9, left). The photophysical properties of the polymers could be correlated with the ratio of thienyltriazine unit. The polymers with a low ratio of thienyltriazine, i.e., **P9.1(a-c)** exhibited an absorption maximum around 385 nm localised in the polyfluorene unit and another charge transfer band at 425 nm. This charge transfer band was enhanced for **P9.1 d** due to increased ratio of thienyltriazine. Emission spectra of the polymers also showed two bands in the region 470–500 nm and 410–440 nm attributed to charge transfer and polyfluorene unit, respectively (Figure 7B). All the polymers exhibited TPA activity in the range 600–900 nm. Increase in the ratio of thienyltriazine unit enhances the conjugation length of the polymer, thus making it more planar and rigid which in turn enhances its TPA cross-section.^[97]



Scheme 9. 2,4,6-Tri(thiophen-2-yl)-1,3,5-triazine-based hyperbranched polymers synthesized by varying the monomer concentration.

A similar study in this regard was also reported by a different group, this time by introducing solubilising group to address the solubility issue of the polymers belonging to the P9.1 series. Thus, a hexyl group was introduced into the thienyl group and two series of polymers P9.2 and P9.3 were synthesized by tuning the donor and acceptor ratios. In the P9.2(a–h) series, the alkyl substitution on the thienyl unit is closer to the triazine core and in P9.3(a–f), the same is closer to the fluorene bridge (Scheme 9, right). The polymers displayed much more enhanced solubility and higher number-average molecular weight. Increasing the ratio of the triazine unit leads to enhanced nonlinear absorption property but a decreased quantum yield. The position of alkyl group also influenced the TPA cross-section. Substitution at the β -position of the thienyl group closer to the triazine unit favours nonlinear absorption in the P9.2(a–h) series when compared to the P9.3(a–f) series. This report showed a new dimension to influence the TPA property of thienyltriazine-containing polymers.^[98]

3.3 Thienyltriazine-based porous systems

Porous organic polymers (POPs) are an emerging class of materials that offer several advantages over their inorganic counterparts such as high specific surface areas, low densities, tuneable porosities, high chemical and thermal stabilities, easy post-functionalization, variable compositions, extended conjugation etc. Besides that, heterocyclic systems are very com-

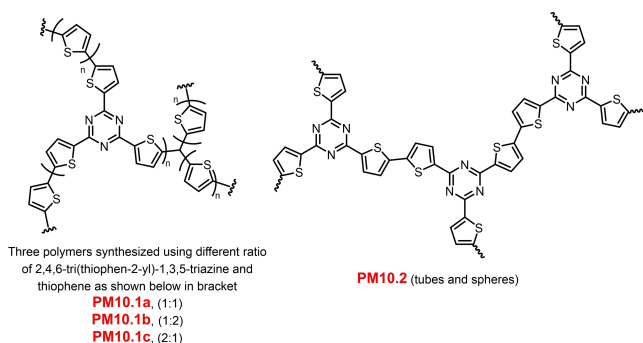
monly employed in the synthesis of POPs and thus the high content of atoms like nitrogen, sulfur, oxygen, and other non-metallic atoms make them ideal candidates for various applications. POPs are generally classified into four types: Conjugated microporous or porous polymers (CMPs or CPPs), hyper-crosslinked polymers (HCPs), covalent organic frameworks (COFs) and covalent triazine frameworks (CTFs).^[99] Besides that, POPs are becoming attractive candidates for applications in diverse fields such as gas storage, photocatalysis, energy storage, optical devices, biological applications, chemical sensing, water treatment etc.^[100–102] The triazine system is one of the most explored units in POPs, yet the number of publications involving thienyltriazine as a combined system are still scarce despite the potential advantages that it offers. In the following sections, the applications of thienyltriazine-based porous polymers are discussed from different perspectives.

3.3.1 Materials for gas storage

The presence of electron-rich aromatic rings and a large heteroatom content can enhance the host-guest interaction of CPPs and boost their overall performance in gas storage. The thienyltriazine system not only contains the electron-rich thiophene rings but also has a large heteroatom content. It has been thus widely explored for the synthesis of porous materials for gas storage applications.

Kundu and co-workers reported the synthesis of hyper-cross-linked microporous polymers **PM10.1a**, **PM10.1b**, and **PM10.1c** (Scheme 10) by using thienyltriazine and thiophene monomers in the ratio 1:1, 1:2, and 2:1, respectively, in the presence of anhydrous FeCl_3 in chloroform under solvothermal conditions at 150°C . **PM10.1a**, **PM10.1b**, and **PM10.1c** displayed a BET (Brunnauer, Emmett and Teller) surface area of 855, 425, and $566\text{ m}^2\text{ g}^{-1}$ and pore volume of 0.2968, 0.1920, and 0.1618 cc g^{-1} , respectively. These polymers had excellent thermal stability and showed highly efficient Lewis-acidic CO_2 adsorption attributed to the presence of electron-donating N and S sites in the polymer backbone. A high CO_2 uptake in the range $10.5\text{--}14.3\text{ mmol g}^{-1}$ and $1.9\text{--}2.6\text{ mmol g}^{-1}$ was observed at 273 K and 298 K, respectively. Despite the medium surface area of **PM10.1c**, it showed the highest CO_2 adsorption ascribed to the highest N and S content present in the polymer. The presence of the triazine ring imparts the polymers with high Qst values but yet these were lower than the energy of chemical bond formation. The calculated CO_2/N_2 selectivities of **PM10.1a**, **PM10.1b**, **PM10.1c** were 72:1, 70:1, and 23:1, respectively, at 273 K.^[103]

Wang and co-workers reported the Ni^0 -catalysed synthesis of tubular porous organic polymer **PM10.2** (Scheme 10) by



Scheme 10. 2,4,6-Tri(thiophen-2-yl)-1,3,5-triazine-based porous materials for gas storage applications.

using a Yamamoto-type Ullmann coupling reaction.^[104] This reaction employs dimethylformamide (DMF) as solvent with 2,2'-bipyridyl as an acid receptor. It is proposed that nanocrystals like quaternary ammonium salts can be formed in-situ by the quaternisation of 2,2'-bipyridyl in presence of halogen compounds. Hence, on using an equivalent amount of 1,2-dibromomethane and $[\text{Ni}(\text{cod})_2]$ against 2,2'-bipyridyl, generation of tubular networks of **PM10.2** was observed and 0D ball-like structures were realised by adopting the same procedure in absence of 1,2-dibromoethane (Figure 8A–F). The tubular CMPs also exhibited very high pore volume of around 1.07 cc g^{-1} , surface area of around $741\text{ m}^2\text{ g}^{-1}$ and high CO_2 adsorption enthalpy of around 40.3 kJ mol^{-1} . The nanosphere CMPs had a slightly higher CO_2 uptake compared to the tubular networks which was attributed not only to the large pore volume but also to the easy diffusion of CO_2 into the nanospheres. The polymer networks also displayed an excellent CO_2 selectivity over N_2 even at low loading of CO_2 making them ideal candidates for CO_2 sequestration.

The influence of varying the linker between the thienyltriazine units on the electronic and gas adsorption properties was studied by Kumar and co-workers by synthesis of four porous polymers **PM11.1** (obtained by an alkyne cyclotrimerization reaction), **PM11.2** (obtained by a Sonogashira coupling reaction), **PM11.3** (obtained by a Glaser coupling reaction) and **PM11.4** (obtained by a Stille coupling reaction).^[105] Varying the spacer between the thienyltriazine units resulted in highly efficient tuning of the properties. The BET surface area was found to be 545, 511, $491\text{ m}^2\text{ g}^{-1}$, the pore size was found to be 3.6, 4.8, and 5.3 nm and the band gap values were found to be 2.43, 2.11, and 2.03 eV, for **PM11.1**, **PM11.2**, and **PM11.3**, respectively. The trend of the BET surface area and pore size can be attributed to the increasing size of the linker whereas the trend of band gap is in accordance with the extent of conjugation. The pore size distribution indicates the dominance of mesopores and macropores arising from interparticular voids in the polymer frameworks. Polymer **PM11.1** was earlier reported by Wang and co-workers by direct-arylation

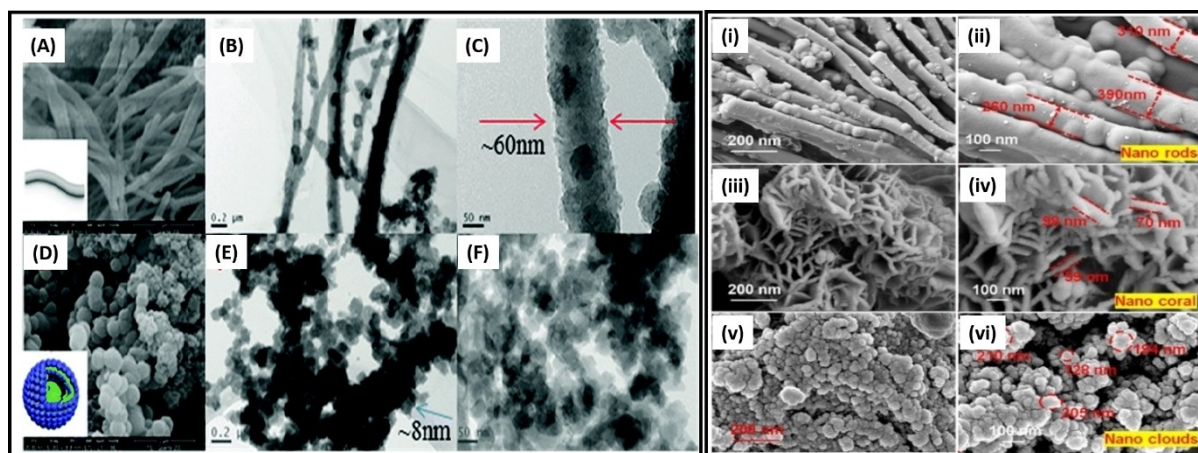


Figure 8. SEM image (A), TEM image (B) and HR-TEM image (C) of tubular **PM10.2**; and SEM image (D), TEM image (E), and HR-TEM image (F) of ball-like **PM10.2**. Reproduced with permission from Ref. [104]. Copyright Royal Society of Chemistry, 2017. FE-SEM images of **PM11.4** (i, ii), **PM11.5** (iii, iv) and **PM11.6** (v, vi), respectively, with different morphologies. Reproduced with permission from Ref. [106]. Copyright American Chemical Society, 2022.

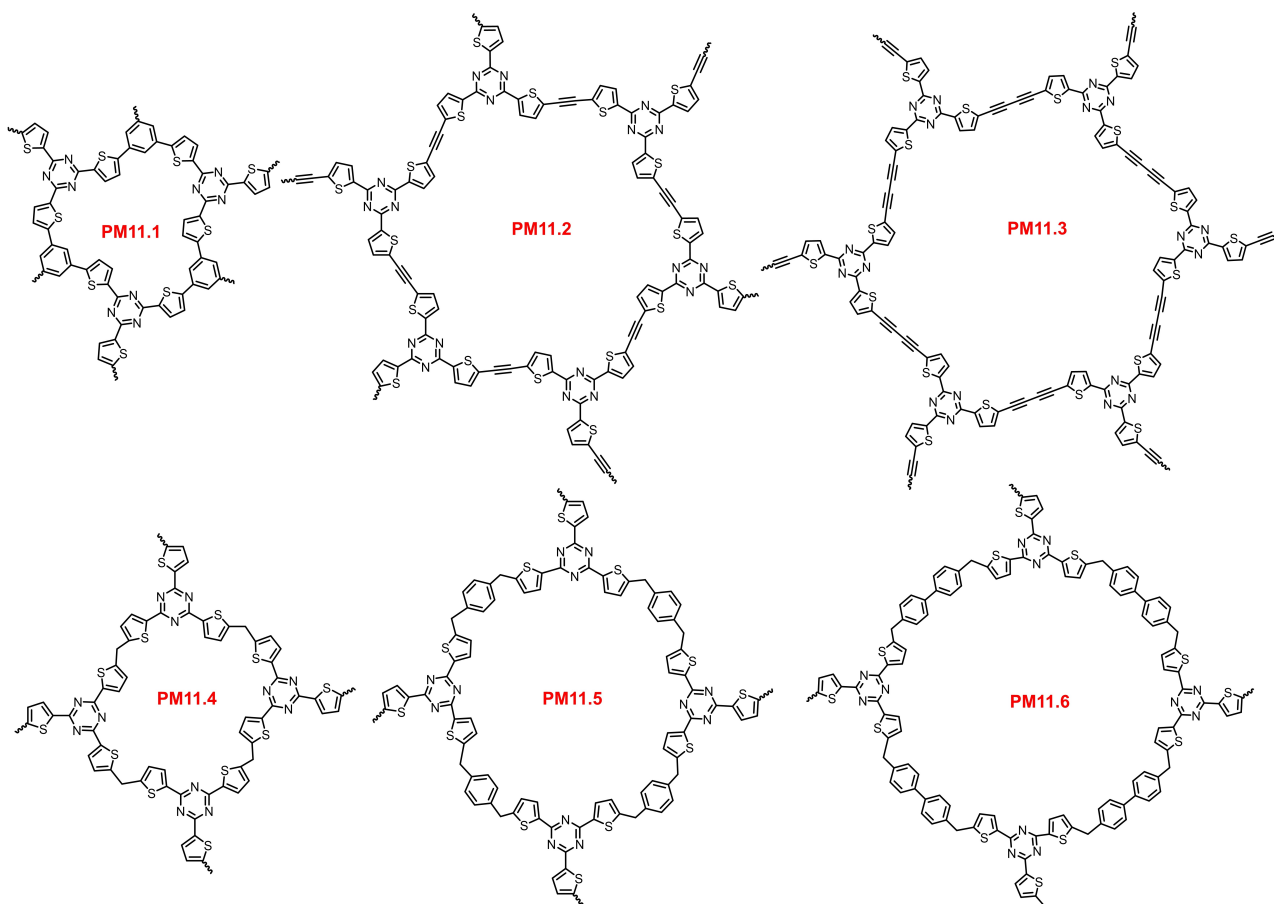
polymerization,^[104] and changing the reaction condition as detailed in the report by Kumar and co-workers led to a 2.5-fold increase of the surface area. Besides that, a change in morphology from fibrous to spherical particle type was also observed. The high heteroatom content of the polymers led to a high CO₂ adsorption reaching up to 11.4 wt% (2.6 mmol g⁻¹) at 263 K under 100 kPa for **PM11.1**, attributed mainly to its small pore size and strong adsorbate-adsorbent interactions. Configurational bias Monte Carlo (CBMC) insights revealed strong quadrupole-quadrupole and dipole-quadrupole interactions between the CPPs and CO₂ and a highest binding energy of 30.5 kJ mol⁻¹ was observed for **PM11.1**.

Another report that involved the precise skeleton engineering of the polymer backbone by varying the linkers was reported by Das and co-workers. They synthesized three polymers **PM11.4**, **PM11.5** and **PM11.6** by changing the cross-linking agents from formaldehyde dimethyl acetal to 1,4-bis(bromomethyl)-benzene (BMB) and 4,4'-bis(bromomethyl)biphenyl, respectively (Scheme 11). The precise tuning of the skeleton resulted in nanorod, nanocoral and nanocloud morphologies for **PM11.4**, **PM11.5**, and **PM11.6**, respectively [Figure 8(i-vi)]. The 2D nanocoral morphology of **PM11.5** and 3D nanocloud morphology of **PM11.6** were attributed to the absence of π - π stacking interaction between the polymer backbones due to presence of electron-rich cross-linking units

and the 1D nanorod morphology of **PM11.4** arose from π - π stacking interaction between the polymer backbones due to the small size of the linker. **PM11.4**, **PM11.5** and **PM11.6** displayed high BET surface areas of 258, 368, and 974 m² g⁻¹ and high CO₂ uptakes of 33.04, 40.06, and 34.12 cm³ g⁻¹, respectively, at 273 K. Interestingly, **PM11.5** bearing a BMB linker had the highest CO₂ uptake both at 298 and 273 K in comparison with the other polymers. This was attributed to the more polarized interaction of CO₂ with the thiophenyl and benzyl rings compared to the N and S atoms in **PM11.5** which resulted in an enhanced CO₂ uptake capacity with respect to the other polymers. Moreover, the E_{bind} for the CO₂ interactions at the thiophenyl and benzyl rings were more negative for the polymer **PM11.5** (i.e., -19.5 and -18.2 kJ mol⁻¹, respectively) than the ones for the **PM11.6** structure (i.e., -19.1 and -16.4 kJ mol⁻¹, respectively).^[106]

3.3.2 Materials for removal of metal-ions

Several techniques such as precipitation, membrane filtration, ion-exchange, adsorption etc. are employed for the removal of toxic metal ions from waste water.^[107-113] Adsorption by porous organic solids is turning out to be an economically viable and efficient method in this direction. Functionalities that show



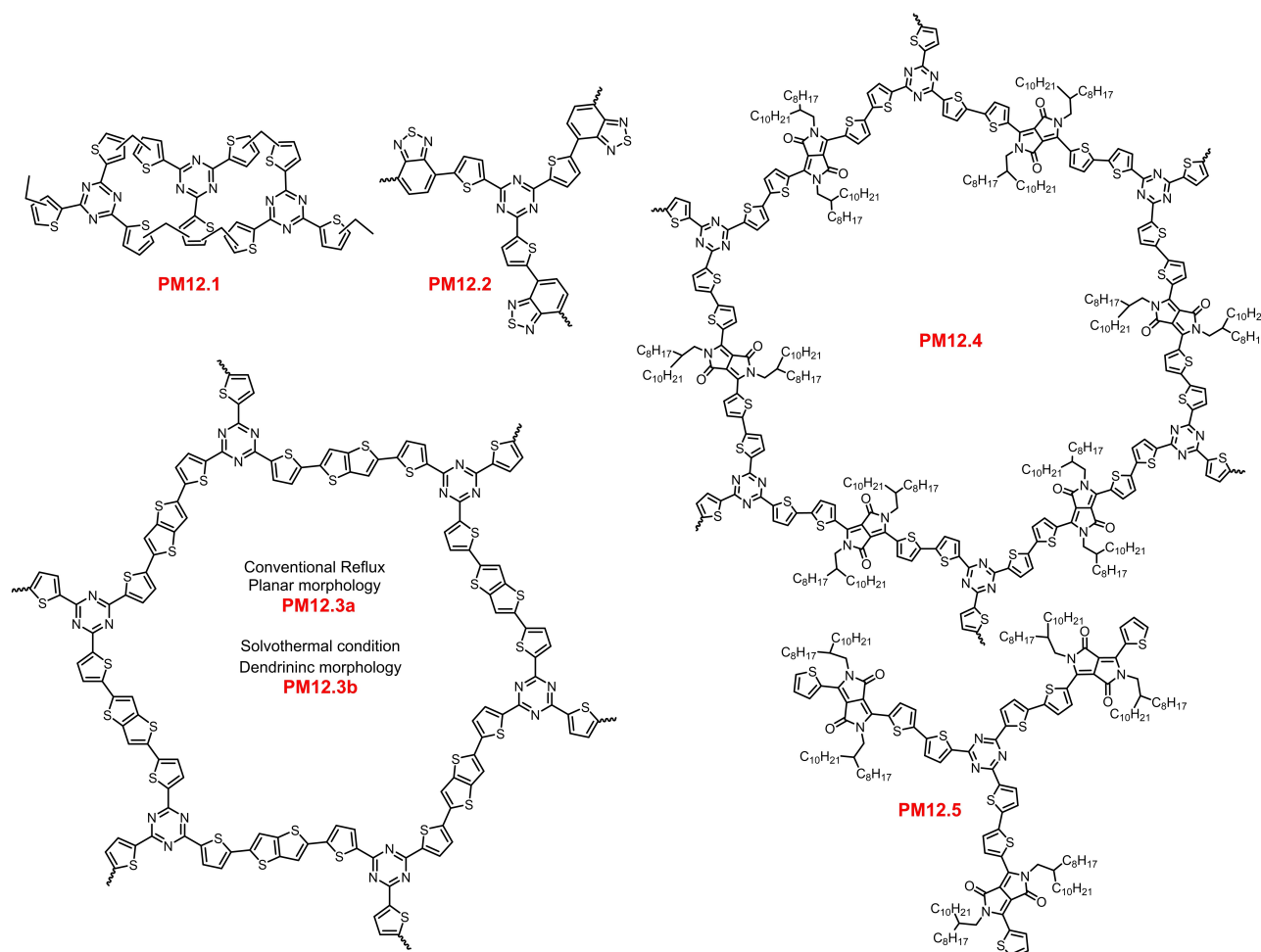
Scheme 11. 2,4,6-Tri(thiophen-2-yl)-1,3,5-triazine-based porous materials for gas storage applications.

enhanced interaction with metal ions like heteroatoms, alkyne functionalities etc. can be easily introduced and task-specific materials with versatile applications can be designed.^[114–117] Thienyltriazine-containing porous materials have been explored in this regard.

He and co-workers reported a task-specific porous polymer **PM12.1** obtained from a Friedel–Crafts reaction between thienyltriazine and dimethylacetal (Scheme 12). This polymer had a decent surface area of around $255 \text{ m}^2 \text{ g}^{-1}$ and pore size of 1 nm and 3 nm. Morphological analysis revealed hollow tubes with 300 nm thickness of the wall and inner diameters of 400 nm. **PM12.1** was very efficient in removing Cu^{2+} ions from aqueous solutions with a maximum adsorption capacity of 98.33 mg g^{-1} as determined by using the Langmuir model. Experimental and theoretical insights revealed that the N and S heteroatoms of **PM12.1** can form coordination complexes with Cu^{2+} which supports the efficiency of **PM12.1** in removing Cu^{2+} from its aqueous solution (Figure 9A). Besides that, covalent interactions like electron delocalization can also enhance the Cu^{2+} adsorption process. **PM12.1** had a high adsorption capacity for Cu^{2+} ions compared to other dipositive ions like Pb^{2+} , Zn^{2+} , Ni^{2+} , Co^{2+} etc. Besides that, the polymer was easily

recycled without any loss in its adsorption capacity. Computational insights revealed the binding energy of the **PM12.1**- Cu^{2+} complex to be around $-1229.64 \text{ kJ mol}^{-1}$, indicating the presence of strong interactions (Figure 9B).^[118]

Another thienyltriazine- and benzthiadiazole-containing polymer **PM12.2** synthesized by a Suzuki coupling reaction was used for the selective sensing of Fe^{3+} ions (Scheme 12).^[119] The polymer exhibited a surface area of $185 \text{ m}^2 \text{ g}^{-1}$, a pore size of 1.4 nm and a total pore volume of $0.54 \text{ cm}^3 \text{ g}^{-1}$. Furthermore, it exhibited excellent thermal stability at up to 600°C . The polymer displayed fluorescence in DMF solution. The selective sensing of **PM12.2** towards Fe^{3+} ions was confirmed by fluorescence studies where it was observed that addition of Fe^{3+} ions resulted in quenching of fluorescence and the fluorescence could be recovered in a facile manner upon the addition of tetrabutylammonium fluoride. Polymer **PM12.2** can selectively detect Fe^{3+} ions in presence of other metal ions like Li^+ , Na^+ , Mg^{2+} , Ba^{2+} , Al^{3+} , Pb^{2+} , Cr^{3+} , Fe^{3+} , Co^{2+} , Ni^{2+} , Cu^{2+} , Ag^+ , Zn^{2+} , Cd^{2+} ($2.5 \times 10^{-3} \text{ mol L}^{-1}$) or other counter ions. Insights into the photophysical property and XPS analysis revealed that electron transfer from **PM12.2** to the vacant d orbitals of Fe^{3+} and interaction between Fe^{3+} and nitrogen centre could the



Scheme 12. 2,4,6-Tri(thiophen-2-yl)-1,3,5-triazine-based porous materials for removal of metal ions and (**PM12.1** and **PM12.2**) and photovoltaic materials (**PM12.3**, **PM12.4** and **PM12.5**).

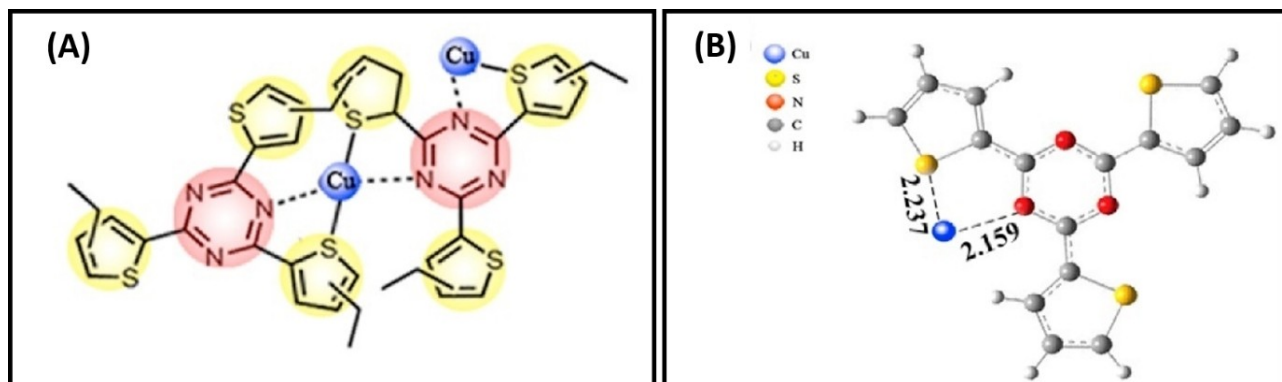


Figure 9. (A) Illustration of chelating interactions between Cu^{2+} and triazine and thiophene groups in **PM12.1**. (B) Optimized geometries and the interactions between **PM12.1** and Cu^{2+} using the DFT B3LYP method. Reproduced with permission from Ref. [118]. Copyright Elsevier, 2016.

cause of fluorescence quenching. The detection limit for Fe^{3+} was found to be $0.78 \mu\text{M}$.

3.3.3 Materials for photovoltaic applications

The application of conventionally synthesized porous organic materials as active materials in photovoltaic devices is very rare, though electrochemically generated porous polymers are more often explored in devices. Park and co-workers synthesized covalent organic nanosheets (CONs) **PM12.3a** and **PM12.3b** by a Stille coupling reaction using conventional reflux and solvothermal conditions, respectively (Scheme 12). Morphological insights revealed that **PM12.3a** had paper-like morphology, as the conventional refluxing method leads to homogenous diffusion of Pd^0 catalyst equivalently in 2-dimensional direction whereas in **PM12.3b**, a dendronic morphology was observed due to diffusion of the catalyst only by the convection flow of the solution. Electrochemical insights revealed **PM12.3a** and **PM12.3b** CONs to be potential candidates to be explored as hole transport layers (HTLs). The films were cast from DMSO by using both CONs with PEDOT:PSS (PEDOT: poly(3,4-ethylenedioxythiophene), PSS: poly(styrenesulfonate)). The rough morphology of **PM12.3b** resulted in unfavourable hole transport

properties compared to **PM12.3a**. SEM, AFM and XRD analyses revealed CON **PM12.3a** to be a better suited material and the PCE of the optimised devices involving CON **PM12.3a** reached around 10.2% which was around 4% higher than found for devices involving **PM12.3b** (Figure 10A). For **PM12.3a** and **PM12.3b**, V_{OC} values of 0.95 and 0.97 V were found and J_{SC} were recorded to be 16.33 and 14.00 mA cm^{-2} , respectively.^[120]

Fu and co-workers synthesized a solution-processable COF-like material **PM12.4** by a Stille coupling reaction of alkyl chain-substituted dibromo diketopyrrolopyrrole as the acceptor and stannylated thienyltriazine as the donor counterpart (Scheme 12).^[121] The presence of alkyl chains resulted in a very low BET surface area of $5 \text{ m}^2 \text{ g}^{-1}$ for the polymer and a total pore volume of $2.9 \text{ cm}^3 \text{ mg}^{-1}$. Electrochemical insights revealed the HOMO and LUMO of **PM12.4** to be at -5.36 and -3.75 eV , respectively. Also, thin films of the polymer exhibited high crystallinity and efficient transport property making it an ideal candidate to be explored in solar cells. The device architecture of perovskite solar cells using **PM12.4** film as the interlayer is shown in Figure 10B. The optimized device with **PM12.4** layer showed a high V_{OC} of 1.13 V, a J_{SC} of 24.01 mA cm^{-2} and a notable FF of 80.8%, leading to a remarkable PCE of 21.92%, which was among the highest efficiencies reported for perovskite solar cells. The FTIR results successfully confirmed

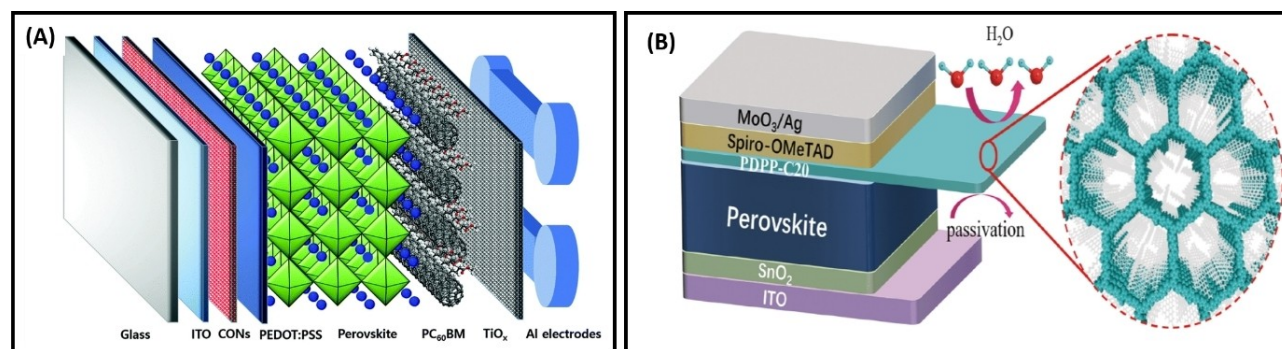


Figure 10. (A) Schematic of the device architecture of the planar-type MAPbI_3 perovskite solar cells (PSCs) involving porous materials **PM12.1** and **PM12.2**. Reproduced with permission from Ref. [120]. Copyright Royal Society of Chemistry, 2018. (B) Device structure of perovskite solar cells using PDPP,C20 (**PM12.4**) film as the interlayer. Reproduced with permission from Ref. [121]. Copyright Springer Nature, 2020.

that the **PM12.4** skeleton containing C=O groups could passivate the surface of perovskite by playing the role of a Lewis base. Thus, the high V_{OC} of devices involving **PM12.4** was believed to be a consequence of an effective hole extraction and less non-radiative carrier recombination sites through suppression of surface Pb defects. The soluble COF-like material **PM12.4** was also explored as donor material in bulk-heterojunction organic solar cells and an efficiency of 2.46% was obtained in this case. This result showed a new group of soluble COF-like materials to be explored in devices.

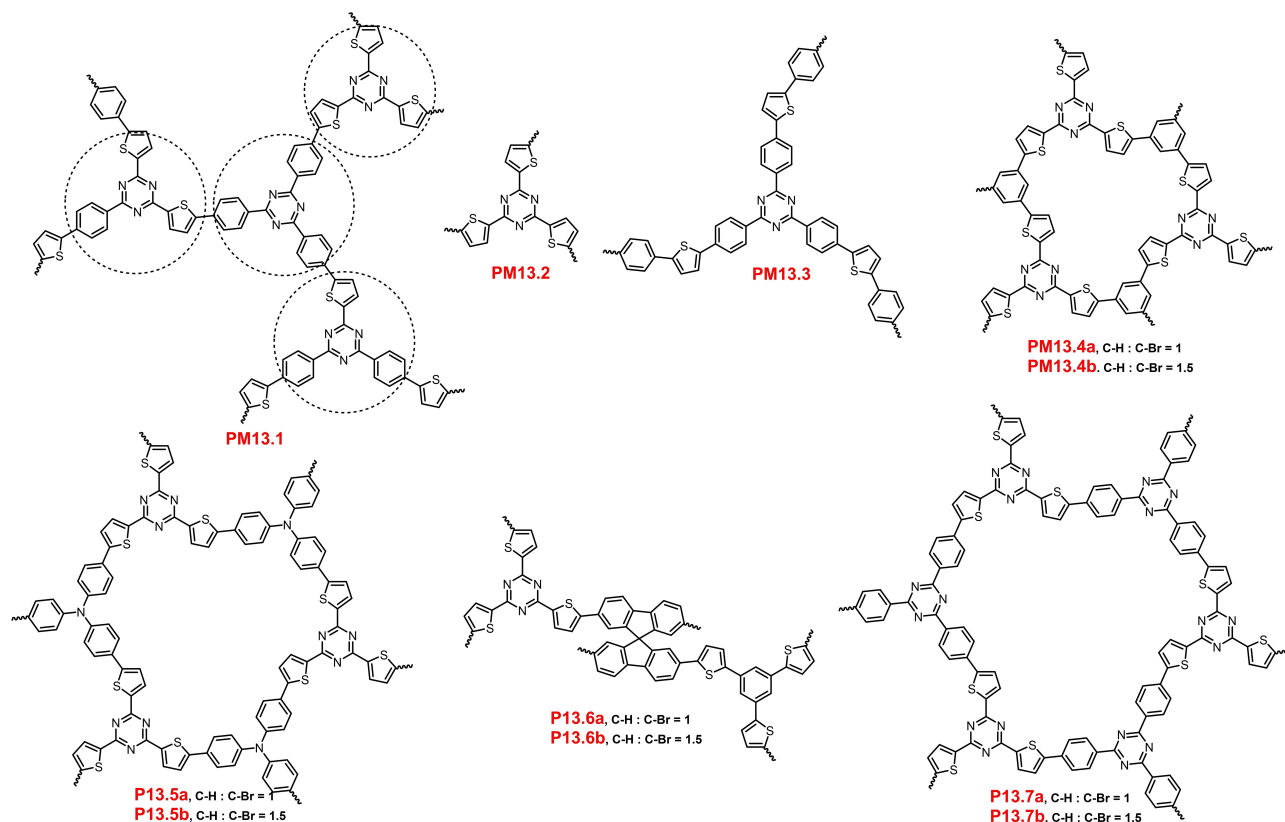
3.3.4 Materials for catalytic and energy storage applications

One of the most interesting and promising applications of POPs that holds a huge potential for the future is in the direction of catalysis and energy storage.^[122] Organic polymers can be built by using task-specific building blocks which can lead to tailoring of properties at will for superior catalytic materials. POPs offer many possibilities to control the structure-activity relationship and their remarkable chemical and thermal stability, high surface area, insolubility etc. make them highly ideal candidates for heterogeneous catalysis.^[123,124] For heterogeneous photocatalytic materials, the performance can be deteriorated due to recombination of photogenerated electron-hole pairs and hence, for POPs, enhanced charge separation and thermodynamically favourable band positions are of utmost importance. Combining donor-acceptor systems that lead

to effective intramolecular charge transfer is an efficient strategy that addresses the aforementioned problem to a large extent and thienyltriazine-containing polymers are appropriate candidates for this purpose.

Huang and co-workers reported the synthesis of three mesoporous CTFs, **PM13.1**, which is asymmetric and consists of four different molecular donor-acceptor domains, and **PM13.2** and **PM13.3** which are symmetric CTFs (Scheme 13).^[125] These polymers had excellent thermal stability up to 500 °C and showed a BET surface area of 52, 78, and 62 m² g⁻¹, respectively. The polymers exhibited a broad adsorption profile extending up to 800 nm and exhibited an optical band gap of 2.30, 2.48, and 2.42 eV for **PM13.1**, **PM13.2**, and **PM13.3**, respectively. The asymmetry in the CTF resulted in an enhanced photogenerated charge separation, intramolecular electron transfer, and a sufficient photoredox potential besides offering a superior performance compared to the symmetric CTFs. The superiority of the asymmetric CTF over the symmetric CTFs containing similar donor and acceptor moieties was proven by the photocatalytic formation reaction of benzophosphole oxides from diphenylphosphine oxide and diphenylacetylene derivatives in 31–95% yield [Figure 11(I)]. CV measurements revealed the LUMO to be at -1.30 V, -1.02 V and -1.24 V and the HOMOs to be at +1.0 V, +1.46 V and +1.18 V for **PM13.1**, **PM13.2**, and **PM13.3**, respectively, making them ideal candidates for photocatalytic reactions.

Bohra and co-workers synthesized a series of CPPs (**PM13.4**–**PM13.7**, Scheme 13) by direct arylation polymerization of



Scheme 13. 2,4,6-Tri(thiophen-2-yl)-1,3,5-triazine-based porous materials for catalytic applications.

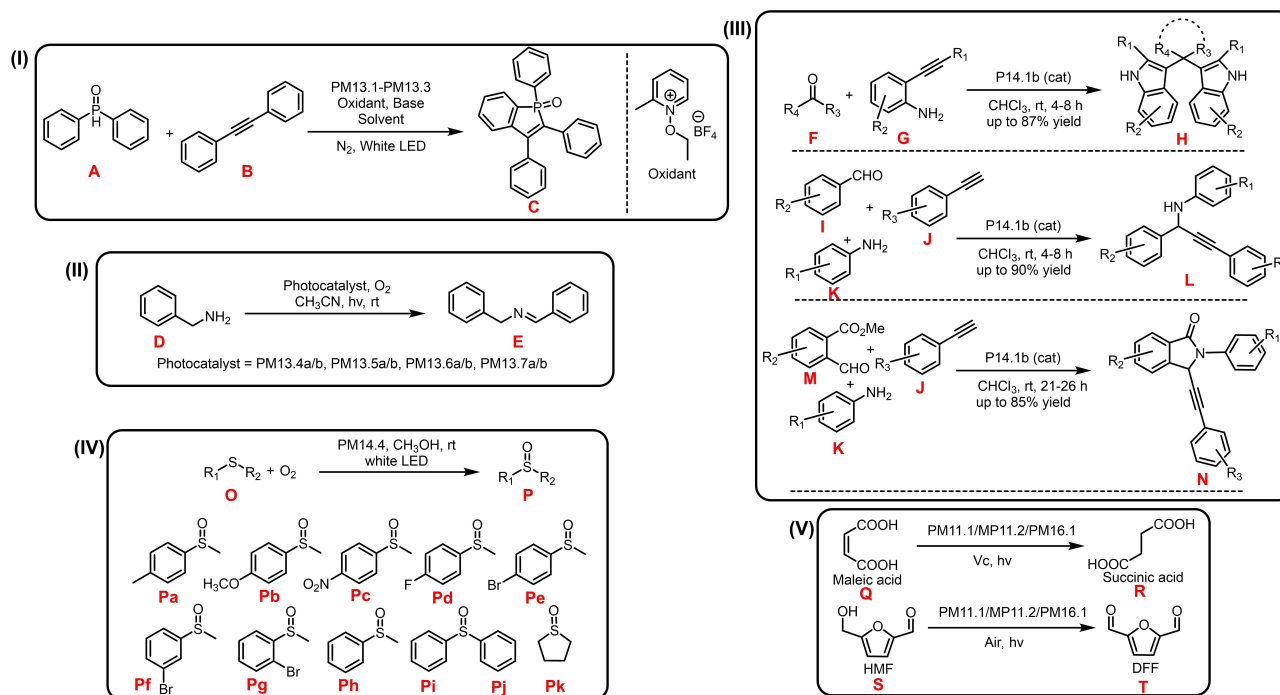


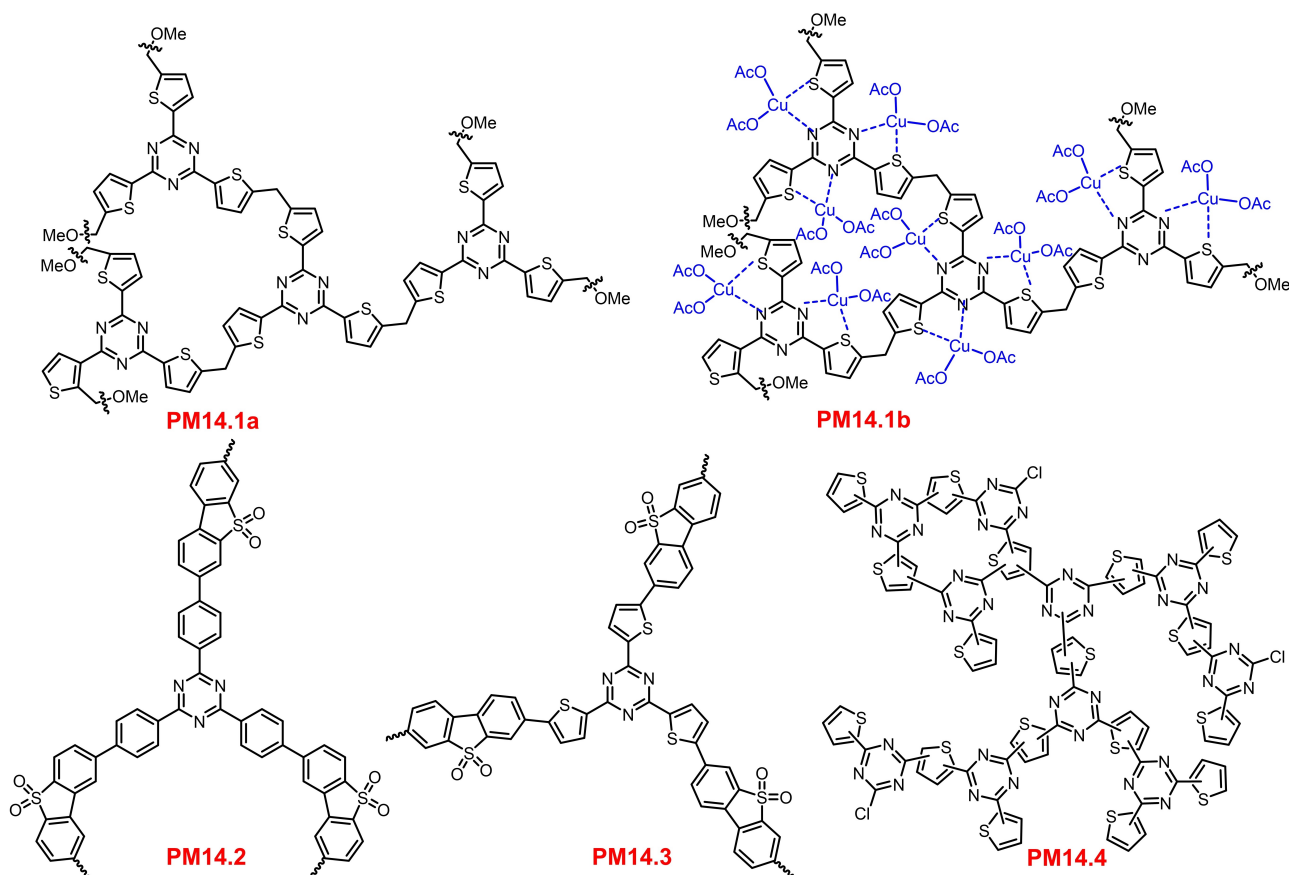
Figure 11. Reactions catalysed by 2,4,6-tri(thiophen-2-yl)-1,3,5-triazine based porous materials.

thienyltriazine with tri- and tetra-brominated aryls using two C–H:C–Br ratios – 1:1 and 1.5:1 with the aim to study the effect of the different geometries and electronic structures of aryl bromides and the effect of varying the molar ratio of a given aryl bromide on the properties of the resultant polymers.^[126] The polymers displayed an excellent thermal stability by retaining 50% of their mass at temperatures as high as 700 °C. Photophysical insights revealed that the rational choice of monomers can be used to tune the optical band gap of the polymers and the band gap of the polymers followed the order **PM13.4** > **PM13.5** > **PM13.6** > **PM13.7**, consistent with the increasing strength of the electron-donating groups of the comonomers. The choice and molar ratio of the comonomer had a profound effect on the morphology of the polymer. The morphology varied from fibre bundles to featureless aggregates and **PM13.5b** exhibited a morphology that evolved from non-uniform fibrillar structures to well defined bundled nano-fibres over the course of the reaction. Interestingly, increasing the molar ratio of C–H:C–Br from 1:1 to 1.5:1 leads to an increase in surface area in **PM13.4** and **PM13.7**-type polymers, but not for **PM13.5** and **PM13.6** and in these cases, no reliable comparison of pore sizes was obtained. The authors believed that DAP reaction conditions led to formation of an interpenetrated polymer network which inhibited the accessibility of the microporous structures to sorbents such as N_2 gas. Selective oxidation of benzylamine to *N*-benzyl-1-phenylmethanamine was used as a model reaction to demonstrate the photocatalytic activity of triazine-core CPPs involving a catalyst loading of 6 $mg\ mol^{-1}$ [Figure 11(II)]. The superior performances of **PM13.7a** and **PM13.7b** were attributed to the higher content of pyridinic nitrogen in the polymer structure, arising

from the triazine rings in the monomers, whereas the low activity of **PM13.5a** and **PM13.5b** was due to their higher HOMO level (lower oxidation potential) with respect to benzylamine which inhibited the oxidation reaction.

Kundu and co-workers reported the synthesis of a POP, **PM14.1** by using the Friedel–Crafts reaction of 2,4,6-tri(thiophen-2-yl)-1,3,5-triazine and formaldehyde dimethyl acetal in the presence of anhydrous $FeCl_3$, and further treating the polymer with $Cu(oAc)_2 \cdot H_2O$ to prepare the potential catalyst **PM14.1b** (Scheme 14). Morphological insights revealed the width of the fibres of **PM14.1a** and **PM14.1b** to be in the range of 20–35 nm and 20–30 nm, respectively. The BET surface areas of **PM14.1a** and **PM14.1b** were 466 and 395 $m^2\ g^{-1}$, respectively, with a super-microporous character characterised by pore sizes of 1.55 nm and 1.50 nm, respectively. ICP-MS analysis revealed the catalyst loading to be around 2.76 wt% and XPS analysis revealed N and S to be the sites for co-ordination with Cu^{2+} ions. This catalyst was explored for different C–C and C–N coupling and cyclization reactions. The polymer catalyst **PM14.1b** was successfully used for a wide variety of organic catalytic transformations under mild conditions to directly afford valuable diindolylmethanes and spiro-analogues (in yields >80%), phthalimidines (in yields >80%), propargyl amines (in yields >85%), and their sugar-based chiral compounds with high yields using readily available substrates (Figure 11(III)). The catalyst was also easily recycled keeping its chemical stability intact and revealed almost same loading of 2.73 wt% even after the 6th catalytic cycle.^[127]

Wang and co-workers synthesized polymers **PM14.2** and **PM14.3** using phenyltriazine and thienyltriazine with dibenzo[*b,d*]thiophene sulfone (DBTSO) by using a Suzuki



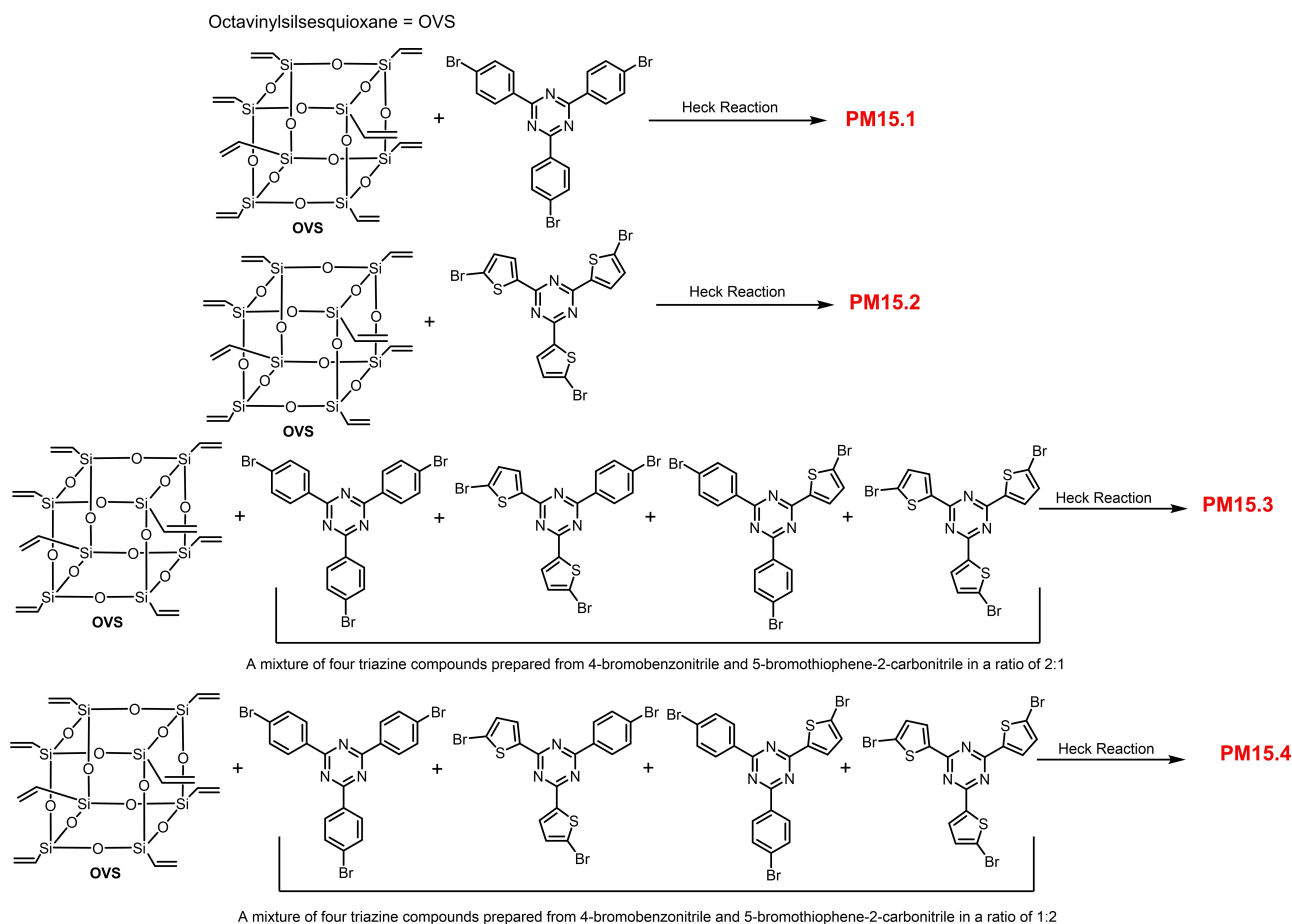
Scheme 14. 2,4,6-Tri(thiophen-2-yl)-1,3,5-triazine based porous materials for catalytic applications.

coupling reaction (Scheme 14).^[128] DBTSO is a strongly electron-withdrawing, planar moiety and because of its hydrophilicity is believed to be an interesting candidate for designing materials with superior hydrogen evolution reaction (HER) activity. The BET surface area of the polymers was found to be $222 \text{ m}^2 \text{ g}^{-1}$ and $48 \text{ m}^2 \text{ g}^{-1}$ for **PM14.2** and **PM14.3**, respectively. The electron-rich nature of the thiophene unit led to a red-shifted absorption of **PM14.3** compared to **PM14.2**. Both CPPs could efficiently separate and transport photogenerated electrons and showed remarkable solar photocatalytic hydrogen evolution ability. **PM14.2** exhibited a HER activity of $16287 \mu\text{mol g}^{-1} \text{ h}^{-1}$ with a quantum yield of 61.5% at 365 nm on irradiation with a 300 W Xe lamp. Under visible light irradiation, a moderate HER activity of $3502 \mu\text{mol g}^{-1} \text{ h}^{-1}$ was found. **PM14.3** exhibited a HER activity of $79 \mu\text{mol h}^{-1}$ ($8776 \mu\text{mol g}^{-1} \text{ h}^{-1}$) under full-spectrum solar irradiation, and a HER activity of $40 \mu\text{mol h}^{-1}$ ($4432 \mu\text{mol g}^{-1} \text{ h}^{-1}$) under visible light irradiation. The lower HER activity of **PM14.3** was attributed to its low surface area and the authors envisioned that enhancing the surface area will directly lead to an enhancement of its activity.

Lan and co-workers synthesized a heterojunction photocatalyst, **PM14.4**, by in situ growth of boron nitride (BN) on donor-acceptor type thienyltriazine-based porous polymer (Scheme 14). Four samples with different loading of boron nitride were synthesized (32 mg, 54 mg, 108 mg, and 214 mg).

XPS analysis revealed that B atoms of boron nitride and N atoms of the porous polymer interacted with each other. This polymer with a cotton-like microspherical morphology displayed very low surface area due to more crosslinked structure caused by boron nitride which resulted in aggregation into a larger network and a resulting shrinking of pores and, secondly, boron nitride probably filled and blocked the pores. Detailed studies were performed using the polymer with the 54 mg loading of boron nitride. Incorporation of BN into the polymer framework improved the light-harvesting property of the polymer besides narrowing its band gap. As negatively charged BN can attract photogenerated holes from the surface of the polymers, the separation efficiency and interfacial transfer rate of photogenerated charge carriers of the porous polymer were significantly improved. A visible-light illuminated superior photocatalytic activity for the metal-free selective oxidation of sulfides was obtained for **PM14.4** [Figure 11(IV)]. Mechanistic studies revealed that the photogenerated electrons reduced O_2 to $^{\bullet}\text{O}_2^-$ radicals and further triggered this oxidation process.^[129]

Du and co-workers designed and synthesized four triazine-functionalized silsesquioxane-based hybrid porous polymers (**PM15.1**, **PM15.2**, **PM15.3** and **PM15.4**) by a Heck reaction of octavinylsilsesquioxane (OVS) with brominated phenyl- or thiophene-substituted triazine monomers using NaHCO_3 as base (Scheme 15).^[130] These hybrid polymers exhibited high specific surface areas of 555, 366, 390 and $364 \text{ m}^2 \text{ g}^{-1}$ for



Scheme 15. 2,4,6-Tri(thiophen-2-yl)-1,3,5-triazine-based porous materials for catalytic applications.

PM15.1, **PM15.2**, **PM15.3**, and **PM15.4**, respectively, and pore volumes 0.55, 0.34, 0.44, and 0.40 cm^3g^{-1} . The enhanced porosity of these materials was attributed to the highly rigid structures of the conjugated aromatic networks and cage silsesquioxanes which prohibited space-efficient packing in solid state. The CO_2 generated in situ during the Heck reaction also increased the porosity. From TGA, three decomposition stages were observed for the polymers, the first at around 300 °C due to loss of moisture, the second around 400 °C due to decomposition of organic functional groups and the third between 600 to 800 °C due to the rupture of the siloxane frameworks. **PM15.1** and **PM15.2** had narrow band gaps of 1.7 eV and 1.5 eV, respectively. The materials showed high photocatalytic activity for the degradation of both acidic and basic dyes (Safranin T, Congo red, rhodamine B and methylene blue) without the requirement of an additional oxidizing agent or any pH adjustment. On exposure to normal light and keeping the concentration of the polymer as low as 0.2 mg mL^{-1} , dyes with a concentration of up to 1000 ppm can be completely decolorized. The polymer also showed a good recyclability. The valence band potentials of **PM15.1** and **PM15.2** were found to be lower than the oxidation potential of $\text{OH}^-/\cdot\text{OH}$ (+2.40 eV) and their conduction band potential was more negative than the reduction potential of $\text{O}_2/\cdot\text{O}_2^-$ (-0.046 eV). This made it

evident that the photogenerated electrons of the porous systems can generate $\cdot\text{O}_2^-$ which triggered the degradation process of the dyes (Figure 12A).

Chen and co-workers reported the design and synthesis of thienyltriazine-containing CMPs with different benzene derivatives, that is, benzothiadiazole, benzene and dimethoxybenzene as linkers, to give **PM12.2**, **PM11.1** and **PM16.1** by a direct arylation reaction. While **PM11.1** presented a 1D nanofiber morphology, the other two polymers had nonuniform bulk particle morphology probably arising from the negative effect of side groups in benzothiadiazole and dimethoxybenzene on π - π stacking interaction which made **PM11.1** to grow faster along the Z direction. The three polymers had decent surface areas of 6, 307 and 39 m^2g^{-1} and optical bandgaps of 2.01, 2.50, and 2.33 eV, respectively. These polymers were explored for photocatalytic conversion of biomass-derived chemicals which involved photocatalytic hydrogenation of maleic acid to succinic acid and oxidation of 5-hydroxymethylfurfural to 2,5-diformylfuran [Figure 11(V)]. The highest photocatalytic activity was observed for **PM11.1** with production rates of 4.66 $\text{mmol g}^{-1}\text{h}^{-1}$ for succinic acid and 0.53 $\text{mmol g}^{-1}\text{h}^{-1}$ for 2,5-diformylfuran. The enhanced photocatalytic activity of **PM11.1** was attributed to the favourable surface properties and charge separation. Interestingly, the same photocatalytic activ-

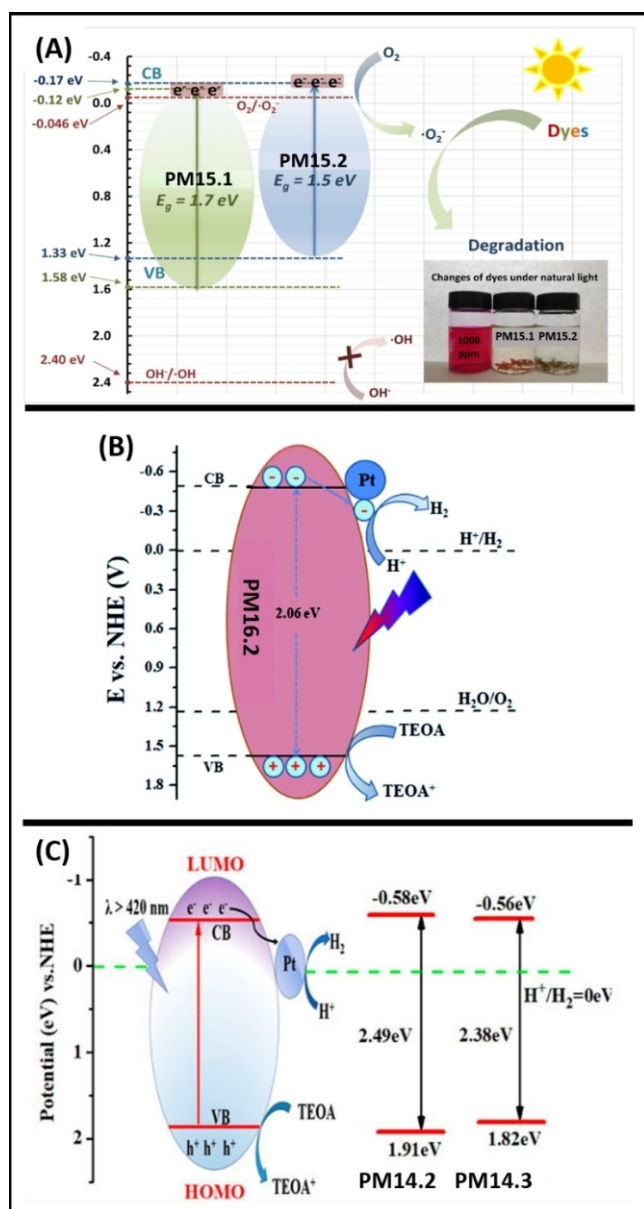


Figure 12. (A) Schematic illustration of the photocatalytic mechanism of dye degradation by PM15.1 and PM15.2. Reproduced with permission from Ref. [130] Copyright John Wiley and Sons, 2021. (B) Photocatalytic mechanism of PM16.2. Reproduced from Ref. [132]. Copyright with the authors of Ref. [132], 2022. (C) Energy diagram and photocatalytic hydrogen evolution mechanism of PM14.2 and PM14.3. Reproduced from Ref. [133]. Copyright with the authors of Ref. [133], 2022

ity was also obtained on irradiation with natural sunlight. The polymers retained their capacity for photocatalytic reaction up to 85% even after five cycles.^[131]

The effect of cross-linker on the photocatalytic activity was studied by Han and co-workers through the synthesis of three CMPs (PM16.2, PM16.3, and PM16.4, Scheme 16) based on thiophenes and triazine by conventional Stille coupling reactions.^[132] The BET surface areas of the three polymers were found to be 138.4, 62.1, 58.8 $m^2 g^{-1}$, respectively, and the optical band gaps were found to be 2.06 eV for PM16.2 and 1.90 eV for PM16.3 and PM16.4, respectively, which could be correlated to

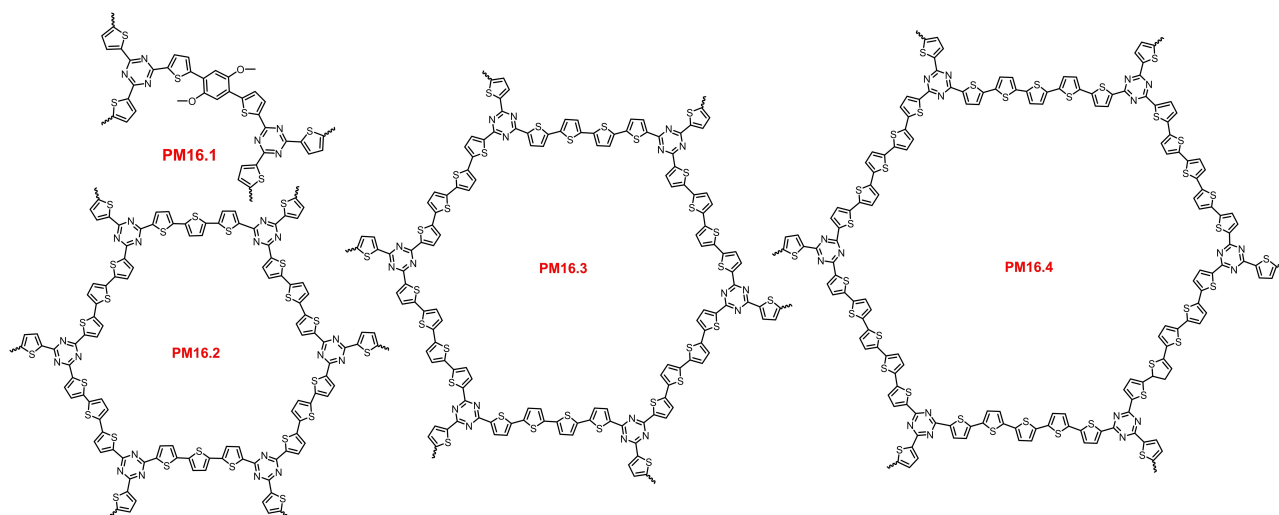
the cross-linker length. PM16.2 showed a higher photocurrent than PM16.4 because of the large specific surface area and small interface charge transfer resistance of PM16.2. Electrochemical studies revealed that all the three polymers were ideal candidates to carry out the water splitting reaction. The polymer with the short cross-linker exhibited the best photocatalytic activity. The activities were found to be 5561.87 $mmol g^{-1} h^{-1}$, 1840.86 $mmol g^{-1} h^{-1}$, and 1600.48 $mmol g^{-1} h^{-1}$ for PM16.2, PM16.3, and PM16.4, respectively. In fact, PM16.2 exhibited a better hydrogen evolution rate than most of the reported triazine-containing polymers. Mechanistic studies revealed that absorption of photons leads to generation of excitons which are transferred to the conduction and valence bands of PM16.2. The heterojunction between PM16.2 and the Pt co-catalyst assisted in splitting the exciton into free charges, thereby further leading to transfer of free electrons to the Pt co-catalyst. These electrons then reacted with H^+ to evolve H_2 directly (Figure 12B).

Polymers PM14.2 and PM14.3 were also separately reported by Sheng and co-workers and explored as photocatalyst for HER. Unlike the previous synthesis reported by Wang and co-workers,^[128] the surface area was smaller in this case with only 54.77 and 22.92 $m^2 g^{-1}$ observed for PM14.2 and PM14.3. The HER photocatalytic activity of PM14.2 was greater than that of PM14.3 and the values were found to be 9,698.5 $\mu mol g^{-1} h^{-1}$ and 4,727.1 $\mu mol g^{-1} h^{-1}$, respectively. The higher activity of PM14.2 was attributed to the higher dipoles of PM14.2 compared to PM14.3, causing a high charge mobility in the former. This leads to a lower recombination rate of electron/hole carriers and higher separation and migration rates for the photogenerated charge carriers. The mechanism of photocatalytic H_2 production is shown in Figure 12C.^[133]

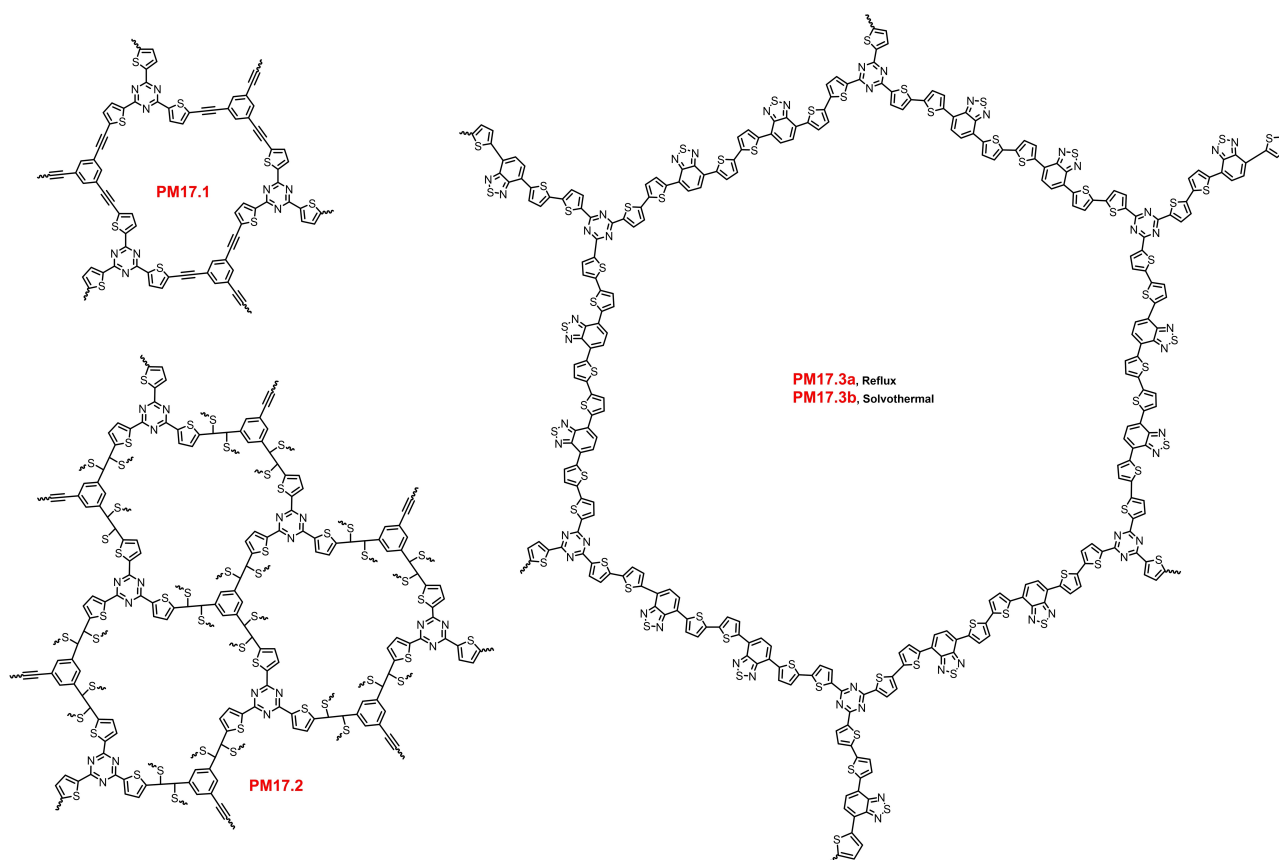
A polymer with backbone same as PM13.2 (Scheme 13) was also synthesized by Xiang and group, employing a nickel-catalysed Yamamoto coupling reaction, and post-synthetic carbonization led to the formation of well-controlled N-doped holey graphitic carbon materials. The carbonized material was explored as a metal-free electrocatalyst for the oxygen reduction reaction (ORR) in fuel cells. This report opened new dimensions in the synthesis of N-doped graphitic structure with precise location control which cannot be obtained with conventional N-doping techniques.^[134]

The highly π -conjugated skeleton, exposed surface area that offers active sites, excellent chemical and thermal stability, structural diversity and designability and low solubility in conventional organic solvents, porous structure to accommodate volume change during charge/discharge process etc. are some of the major factors that make conjugated porous polymers excellent candidate for energy storage applications. This application of thienyltriazine-containing porous materials is one of the most widely explored in current times indicating the huge underlying current potential of such systems.^[135]

Bhosale and co-workers reported the synthesis of microporous polymer PM17.1 through a Sonogashira coupling reaction between thienyltriazine and 1,3,5-triethynylbenzene, resulting in a pore of size 1.3 nm and a BET surface area of 544 $m^2 g^{-1}$ (Scheme 17). This polymer was then carbonized at



Scheme 16. 2,4,6-tri(thiophen-2-yl)-1,3,5-triazine based porous materials for catalytic applications.



Scheme 17. 2,4,6-Tri(thiophen-2-yl)-1,3,5-triazine-based porous materials for energy storage application.

three temperatures (700, 800 and 900 °C) in an inert atmosphere to give **PM17.1@700**, **PM17.1@800**, and **PM17.1@900** with enhanced surface areas of 694, 700, and 624 m²g⁻¹, respectively, compared to the parent polymer. **PM17.1@900** exhibited a capacitance of 211 Fg⁻¹ and the higher storage capacity was due to the increased contribution of graphene. The use of these materials as electrocatalysts to reduce oxygen

was also explored and it is the nitrogen- and sulfur-modulated spin density charge distribution of carbon lattices that enhance the activity of the materials. The number of electrons transferred was found to be in the range 3.3–3.5, which is comparable to that of the theoretical number of electrons transferred (4 e⁻). In the case of **PM17.1@800**, the maximum number of electrons was transferred. The number of electrons

transferred was lowest for **PM17.1@900** at 3.2, probably due to removal of sulphur and nitrogen during the graphitization process at 900 °C.^[136]

The effect of reaction conditions on the designed materials as well as the influence on their energy storage capacity was studied by Kim and co-workers by the synthesis of CONs **PM12.3a** and **PM12.3b** (Scheme 12) by conventional reflux and solvothermal reaction conditions, respectively. The BET surface area of these CONs was determined to be 200 and 300 m²g⁻¹ for **PM12.3a** and **PM12.3b**, respectively. The electrode constructed using **PM12.3b** showed a reversible discharge capacity of ~250 mA h g⁻¹ after 30 cycles at a current density of 100 mA g⁻¹. It also exhibited the best cycling performance and rate capability which was due to its large specific surface area, mass diffusivity and charge-carrier conductivity. The charge storage in **PM12.3a** and **PM12.3b** was largely governed by the diffusion-controlled mechanism. The authors further extended this study by the synthesis of donor-acceptor type CONs **PM17.3a** and **PM17.3b** by incorporating benzothiadiazole along with thienyltriazine (Scheme 17). The former was prepared by reflux conditions and the later by solvothermal conditions. These D/A CONs had band gaps of 1.91 and 1.91 eV and BET surface areas of 160 and 89 m²g⁻¹, respectively. The predicted pore size of materials **PM17.3a** and **PM17.3b** was 4.1 nm. Pore size distributions calculated by the Barrett, Joyner and Halenda (BJH) method revealed that the CONs possessed irregular pores. The solvothermally prepared CON had larger pores compared to the CON prepared under reflux conditions. The previous set of CONs had increased inter-sheet repulsion due to the delocalization of larger negative charges which meant that the D/A CONs were comparatively more exfoliated. The solvothermally prepared D/A CON was used to prepare an electrode which exhibited a highly enhanced reversible discharge capacity (~450 mA h g⁻¹) after 30 cycles at a scan rate of 100 mA g⁻¹. Morphological analysis revealed that floppy and turbostratic assemblies with surface charge induced as a result of incorporation of benzothiadiazole showed better correlation and enhanced correlation with ion mobility.^[137,138]

Liu and co-workers developed a novel sulfur-rich triazine-trithiophene-triacetylenic benzene-conjugated porous polymer cathode material (**PM17.2**) by a covalent linkage between a conjugated porous polymer (**PM17.1**) and sulfur using a radical copolymerization approach (Scheme 17). For 0.2 g of the polymer, around 0.8 g of sulphur were used. The successful incorporation of sulfur at the desired position was confirmed by XPS analysis. TGA analysis revealed a continuous weight loss of the polymer **PM17.2** in the temperature range of 190 to 300 °C attributed to the sublimation of sulfur which covalently connects with **PM17.1**, and the sulfur content was found to be around 80%. Electrochemical studies revealed that the cathodic and anodic peaks had a small gap which confirmed the reversibility of **PM17.2**. An outstanding C-rate capacity at a current rate of 5 C (discharge capacity of 756 mA h g⁻¹) was observed for the cathode material based on **PM17.2**. Even after 650 cycles, a discharge capacity of 440 mA h g⁻¹ with a small decay of 0.055% per cycle was obtained. Furthermore, the Coulombic efficiency of the cell was retained at up to 99.6%

after 400 cycles at 0.5 C. The excellent performance of the sulfur-enriched polymer was ascribed to the prevention of property deterioration due to volume change and also to the effect of an overall conjugated system.^[139]

The use of polymer **PM12.2**, synthesized by Suzuki coupling reaction, in Li⁺ ion storage was explored by Ren and co-workers. The polymer had a specific BET surface area of 100 m²g⁻¹ based on the nitrogen adsorption branch while the same based on carbon dioxide was around 406 m²g⁻¹. Based on the above information, the authors envisioned that the ultramicroporous nature of **PM12.2** would make it an ideal candidate for Li⁺ transport and storage. Besides the richly porous character, the polymer possessed a large number of redox-active units and hence the polymer-derived anode delivered a high Li⁺ storage capacity of up to 1599 mA h g⁻¹ at a current rate of 50 A g⁻¹ with an excellent rate behaviour (363 mA h g⁻¹ at 5 A g⁻¹) and a long-term cyclability of 326 mA h g⁻¹ over 1500 cycles at 5 A g⁻¹. Figure 13(A, B) shows the energy levels and simulated LUMO and HOMO diagrams for **PM12.2** and the schematic diagram of the proposed Li-storage mechanism for the building blocks. The repeating unit of **PM12.2** can accept 27 electrons in total, out of which 12 electrons are transferred into the 1,5-benzothiadiazole unit and 15 electrons are transferred into the thienyltriazine unit. The value calculated using the discharge capacity turned out to be 26.7 which is very close to the theoretically calculated value.^[140]

PM12.2. (B) Schematic diagram of the proposed Li-storage mechanism for the building blocks and (C) the segment of the polymer chain for **PM12.2**. Reproduced with permission from Ref. [140]. Copyright John Wiley and Sons, 2020.

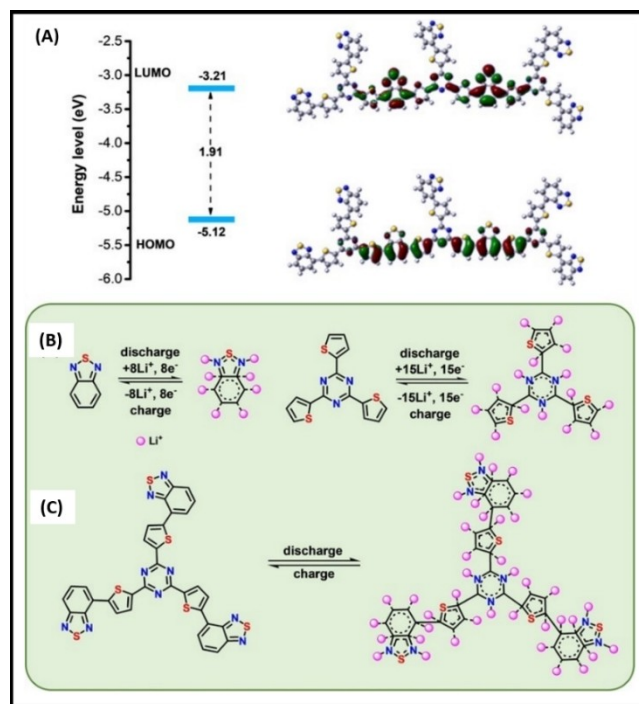


Figure 13. (A) Energy levels for **PM12.2** and simulated LUMO and HOMO diagrams for

Zhang and co-workers prepared thin layers of covalent triazine frameworks (structure similar to **PM13.2** but synthesized via electropolymerization, named as CTF-BTh) containing a bithiophene moiety onto the surfaces of a Cu_2O photocathode and a Mo-doped BiVO_4 photoanode via electropolymerization. Resulting in the generation of hybrid photoelectrodes, this became the first known heterojunction with both photocathodes and photoanodes. Photophysical insights revealed the strong absorption of the polymer up to 550 nm giving it an optical band gap of 2.34 eV as obtained from the Tauc plot. The band structure of CTF-BTh was advantageous to form band edge alignment with each metal oxide leading to a p-n junction and a staggered type-II heterojunction with Cu_2O and Mo-doped BiVO_4 , respectively (Figure 14). The CTF-BTh layer was also used as an anti-photocorrosion layer for both photoelectrodes and enabled the long-term operation for 150 h with only an approximate 10% loss in photocurrent densities.^[141]

Kochergin and co-workers made use of wet chemistry to fabricate polymeric materials on a copper plate that played the role of both surface template and a catalyst. The precursor used was 2,4,6-tris(5-ethynylthiophen-2-yl)-1,3,5-triazine (**3.7**) and the polymer growth was possible via two pathways: (1) Glaser-type polycondensation of terminal alkynes; (2) [2+2+2] cyclo-trimerization of carbon-carbon triple bonds (Figure 15). This meant that the backbones of these polymers, termed as Tz-Th@Cu, were similar to **PM11.1** and **PM11.3**. Tz-Th@Cu showed a moderate BET specific surface area of $42 \text{ m}^2 \text{ g}^{-1}$, a

mesoporous structure with pore sizes in the range of 5 to 25 nm and a narrow band gap of 1.42 eV. However, the [2+2+2] cycloaddition product was expected to have higher energy gaps and the observed band gap related logically with the Glaser-coupled product. This did not rule out the existence of the [2+2+2] product as the narrow band gap of Tz-Th@Cu could be consequence of its D-A composition. The combination of tectons with different electron affinity resulted in a material with a lower band gap, showing an anodic photocurrent density of 6.8 mA cm^{-2} (at 0.6 V vs. Ag/AgCl, pH 7). This value was twice as high when compared to the polymer analogue synthesized by conventional bulk route. On simulated sunlight irradiation, a twofold increase in the photoelectrocatalytic oxygen evolution from water was observed for the prepared electrode with a photocurrent density of up to 4.8 mA cm^{-2} (at 1.0 V vs. Ag/AgCl, pH 14).^[142]

Xue and co-workers studied the effect of linkers of varied length consisting of thiophene units on the capacities of resulting polymers.^[143] The synthesized polymers involved thienyltriazine and different thiophene derivatives including thiophene (Th), thieno[3,2-*b*]thiophene (TT), dithieno[3,2-*b*:2',3'-*d*]thiophene (DTT) or thieno[',3':4,5]thieno[3,2-*b*]thieno[2,3-*d*]thiophene (TTTT) to give polymers **PM16.2**, **PM12.3a**, **PM18.1**, and **PM18.2**, respectively (Schemes 12, 16, and 18). The increase in the size of the linker led to a decrease in the band gap (1.92 eV, 1.83 eV, 1.65 eV and 1.59 eV, respectively) due to higher planarity and an increased conjugation length. The

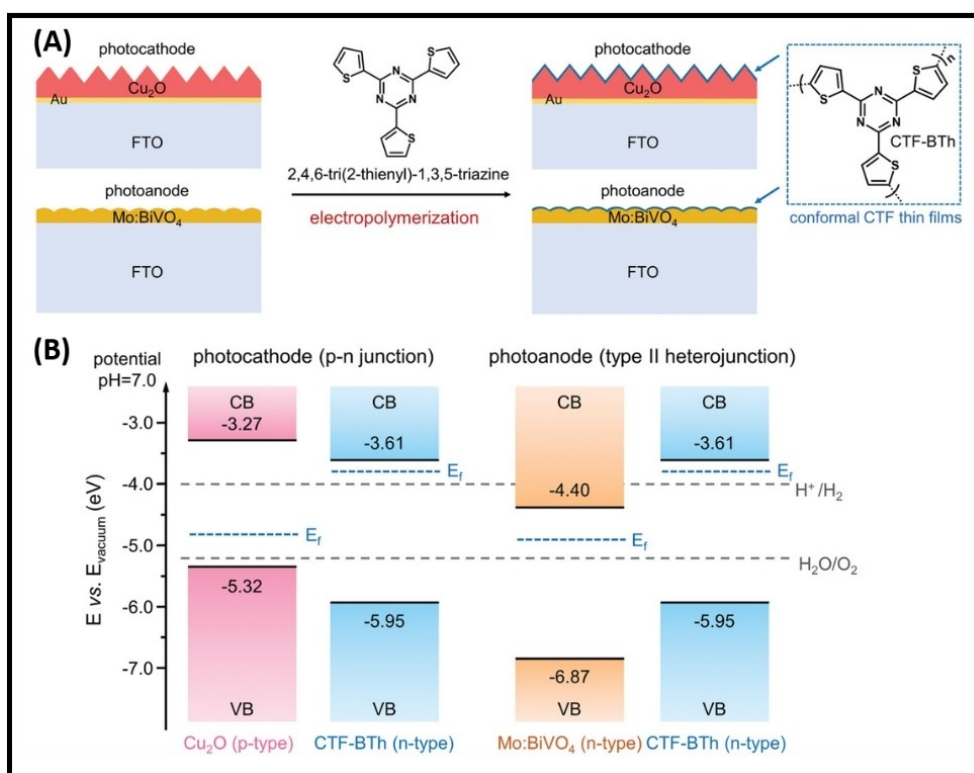


Figure 14. (A) Schematic formation of hybrid CTF-BTh/ Cu_2O and CTF-BTh/ Mo:BiVO_4 photoelectrodes via electropolymerization. (B) Experimentally determined energy diagrams of Cu_2O , Mo:BiVO_4 , and CTF-BTh. The suitable band edge alignments enable the formation of a p-n junction between CTF-BTh and Cu_2O and a staggered type-II heterojunction between CTF-BTh and Mo:BiVO_4 . (The electrochemically grown polymer in this case has a structure similar to that of **PM13.2**). Reproduced with permission from Ref. [141]. Copyright John Wiley and Sons, 2021.

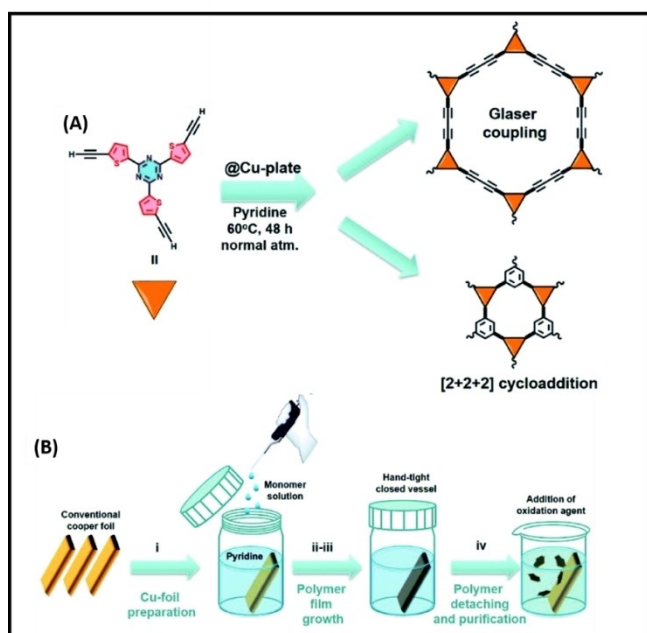
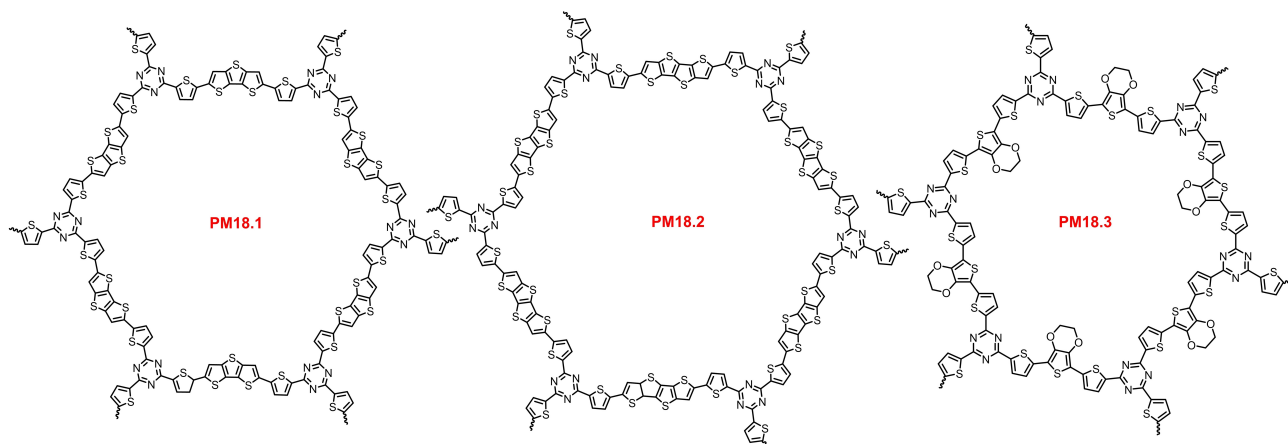


Figure 15. (A) Synthetic pathways towards the preparation of 2,4,6-tri(thiophen-2-yl)-1,3,5-triazine-based polymers on the surface of a conventional copper plate (@Cu plate). (B) Schematic representation of the synthetic procedure that includes (i) preparation of the Cu foil, (ii) submerging of the Cu foil in pyridine and addition of the monomer, (iii) reaction in the hand-tight closed vessel at 60 °C for 48 h, (iv) detaching of the polymer film from the Cu foil with subsequent purification and drying (Glaser-coupled polymer has a framework like **PM11.3** and the [2 + 2 + 2] cycloaddition product has a framework like **PM11.1**). Reproduced from Ref. [142]. Copyright is with the authors of Ref. [142], 2021.

composite materials (polymer@C) between polymers and Vulcan XC-72 carbon were prepared by in situ polymerization to test their electrochemical performances in lithium-ion batteries. Morphological studies revealed the presence of cross-linked structures in **PM18.1@C** and **PM18.2@C** which were prepared from polymers consisting of longer linkers. A longer linker length was associated with a more relaxed intramolecular strain which adorned the materials with a homogeneous morphology.



Scheme 18. 2,4,6-Tri(thiophen-2-yl)-1,3,5-triazine-based porous materials for energy storage applications.

The net-like structures of **PM18.1@C** and **PM18.2@C** proved beneficial to promote ion transport and provided more sites for electrochemical reaction. This was attributed to the penetration of the electrolyte into the net-like structure of the materials. The BET surface areas of the carbonized materials were 79.21, 96.50, 114.46, 120.33 m²g⁻¹, respectively, and the pore sizes were 21.6, 18.41, 17.59, 19.3 nm, respectively. The specific capacities of the composites were found to be 495 mA h g⁻¹, 671 mA h g⁻¹, 707 mA h g⁻¹, and 772 mA h g⁻¹ for **PM16.2@C**, **PM12.3a@C**, **PM18.1@C** and **PM18.2@C** at a current density of 100 mA g⁻¹, respectively.

Chen and co-workers synthesized a triazine-based covalent organic framework, **P18.3** (Scheme 18), by incorporating 3,4-ethylenedioxythiophene (EDOT) as the bridging unit using a Stille coupling reaction in presence of carbon powder. The carbon powder served the purpose of preventing the low intrinsic conductivity of the polymer and led to the in situ formation of polymer composite **PM18.3@C**. The composite had a narrow band gap of 1.84 eV and morphological analyses revealed that small particles agglomerated together to form a porous structure which proved beneficial for use in lithium ion batteries. Electrochemical studies also revealed the favourable redox potential of the composite (1.0 V vs. Li/Li⁺), making it a perfect candidate to be explored as anode material in lithium ion batteries. The composite exhibited a stable specific capacity of 645 mA h g⁻¹ at 100 mA g⁻¹ and 435 mA h g⁻¹ at 500 mA g⁻¹, respectively. These values were significantly higher than those of pure carbon materials.^[144]

Chai and co-workers worked on improving the interfacial microenvironment between the hematite photoanode and cocatalyst to achieve efficient photoelectrochemical water oxidation. α-Fe₂O₃ and Gd-Fe₂O₃ photoanodes were prepared by using hydrothermal and annealing methods. 2,4,6-tri(thiophen-2-yl)-1,3,5-triazine was coated on a Gd-Fe₂O₃ surface by in situ electropolymerization in acetonitrile solution to give a CTF-BTh/Gd-Fe₂O₃ photoanode (CTF-BTh refers to polymers of thienyltriazine). The Co-Sil/Gd-Fe₂O₃ photoanode was prepared by photoassisted electrophoretic deposition (PEPD) in a Co-Sil colloidal solution using a three-electrode

system. The Co-Sil/CTF-BTh/Gd-Fe₂O₃ photoanode was then prepared by sequentially conformally coating the Gd-Fe₂O₃ surface with CTF-BTh and Co-Sil films (Figure 16).

The Co-Sil/CTF-BTh/Gd-Fe₂O₃ photoanode showed an excellent photocurrent density (2.74 mA cm⁻² at 1.23 V_{RHE} [voltage reported against the reversible hydrogen electrode]) and a low onset potential (~630 mV_{RHE}). The modulation effect of CTF-BTh was responsible for improved charge separation and transfer efficiency and allowed the utilization of incident light for α -Fe₂O₃-based photoanodes.^[145]

The literature results discussed above involving diverse emerging applications of thienyltriazine containing materials can lead to plethora of new materials and applications if more efforts are directed in this direction. Thienyltriazine based materials can be of special significance for adopting greener route towards energy storage materials.

4. Conclusion and Outlook

In this review, we have summarized and discussed the advances made in the field of 2,4,6-tri(thiophen-2-yl)-1,3,5-triazine chemistry. This heteroatom-rich C_{3h}-symmetric system consists of a donor-acceptor part, thus making it an interesting candidate in the larger domain of materials chemistry. Its straightforward synthesis involves the cyclotrimerization reaction of 2-cyanothiophene and the tribromo derivative of thienyltriazine is the key intermediate for the synthesis of a wide array of materials. Although triazine and thiophene have previously been explored in diverse fields of materials chemistry, the advances in the chemistry of thienyltriazine system have significantly geared up in the last two decades. The last decade has witnessed improved syntheses as well interesting applications of thienyltriazine-based star molecules and porous materials. Thienyltriazine, as a single unit, offers several advantages such as the inherent donor-acceptor nature,

the high heteroatom content, enhanced supramolecular and π - π interactions with the added benefit of its C₃-symmetry and coplanarity which lead to substantial electronic communication. All these factors make it an ideal candidate to be explored in diverse arenas of organic electronics and porous material chemistry. In fact, researchers across the globe have realized its potential, which has led to new applications of this system in porous materials. The applications of thienyltriazine in the field of catalysis and energy storage are also worth mentioning. Triazine-ring-assisted supramolecular interactions as well as coplanarity-assisted π - π interactions lead to porous materials with unique and controllable morphology to be synthesized easily and hence allow for their applications in fields like gas storage, photovoltaic materials, catalysis and energy storage.

However, to achieve the best performance of thienyltriazine-based star systems and porous materials, some challenges need to be addressed, opening up future directions of research in this field. Some of these challenges and future opportunities include: 1) The triazine-ring-assisted supramolecular interaction, coplanarity-assisted π - π interactions and donor-acceptor nature make the thienyltriazine system an ideal candidate to be further explored for devising ambipolar liquid crystalline materials and ambipolar materials for devices. 2) Exploring environment friendly and cheap reaction pathways for the synthesis of already existing and new systems is the call of the hour. This means to avoid the use of hazardous coupling catalysts which are detrimental to the performance of porous materials in different applications. 3) The non-wettability of porous materials limits their applications and hence strategies to introduce groups that improve the wettability without sacrificing the performance need to be explored. 4) The morphology of porous materials can have a pronounced effect on their gas storage capacity, catalytic activity and energy storage performance. Hence, more efforts are to be focussed on morphology-controlled synthesis of porous materials besides employing template-assisted synthesis. 5) There are several reports that

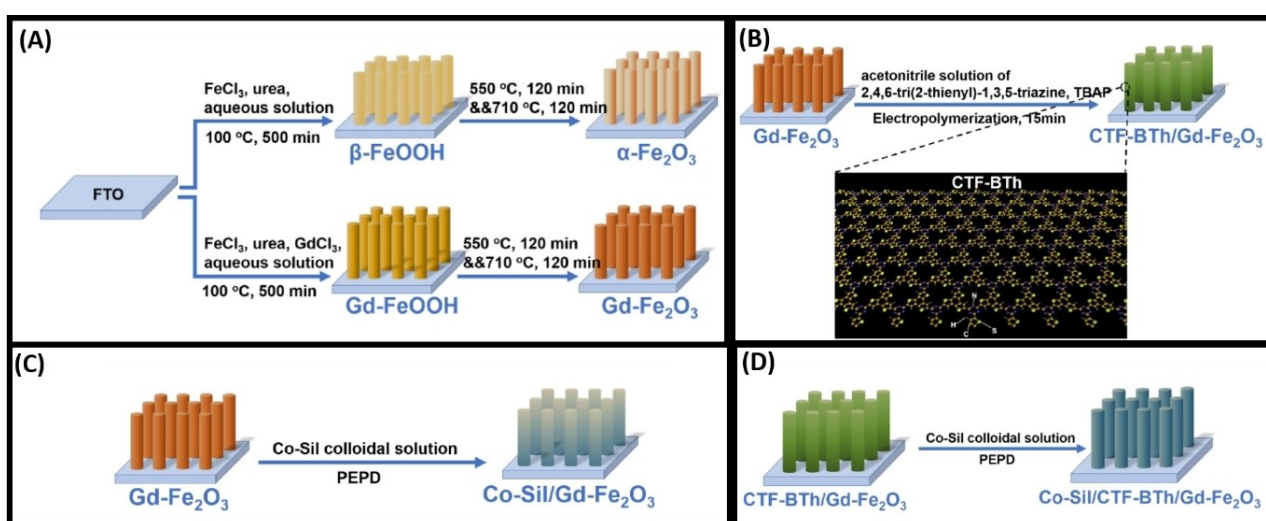


Figure 16. (A) Schematic representation for the preparation of α -Fe₂O₃ and Gd-Fe₂O₃ photoanodes. (B) Schematic representation for the preparation of the CTF-BTh/Gd-Fe₂O₃ photoanode. (C) Schematic representation for the preparation of the Co-Sil/Gd-Fe₂O₃ photoanode. (D) Schematic representation for the preparation of the Co-Sil/CTF-BTh/Gd-Fe₂O₃ photoanode. Reproduced with permission from Ref. [145]. Copyright American Chemical Society, 2022.

prove that the structure of thienyltriazine-based materials has pronounced effects on the performance of the resulting materials. A deeper investigation in this regard like the influence of varied linkers, reaction conditions, monomer ratio, morphology etc. is needed to get detailed insights into the intrinsic relationship of structure, property and performance. 6) Last but not least, incorporation of redox-active moieties, improving the molecular conjugation, high surface area and optimized pore size, formation of oriented films on templates etc. are some challenges that need to be addressed and focussed on for improved performance of thienyltriazine-based energy storage materials.

This review will be of great assistance to materials chemists to design a wide range of thienyltriazine-based systems for advanced applications. Thienyltriazine-based compounds are a promising class of materials that will remain at the forefront of materials chemistry alongside other types of materials and will undoubtedly lead to further landmarks. Further, we hope that this review will act as a catalyst for further exploration of thienyltriazine chemistry and open doors in new directions.

Conflict of Interest

The authors declare no conflict of interest.

Data Availability Statement

Data sharing is not applicable to this article as no new data were created or analyzed in this study.

Keywords: catalysis · energy-storage · porous polymers · star molecules · thienyltriazine

- [1] J. W. Döbereiner, *Ber. Dtsch. Chem. Ges.* **1832**, 3, 141.
 [2] G. Mlostoń, *Chem. Heterocycl. Compd.* **2017**, 53, 1.
 [3] J. A. Joule, *Prog. Heterocycl. Chem.* **2020**, 31, 177–222.
 [4] a) G. Barbarella, L. Favaretto, G. Sotgiu, M. Zambianchi, A. Bongini, C. Arbizzani, M. Mastragostino, M. Anni, G. Gigli, R. Cingolani, *J. Am. Chem. Soc.* **2000**, 122, 11971–11978; b) G. Gigli, O. Inganäs, M. Anni, M. De Vittorio, R. Cingolani, G. Barbarella, L. Favaretto, *Appl. Phys. Lett.* **2001**, 78, 1493–1495; c) M. Pasini, S. Destri, W. Porzio, C. Botta, U. Giovanella, *J. Mater. Chem.* **2003**, 13, 807–813.
 [5] a) R. D. McCullough, *Adv. Mater.* **1998**, 10, 93–116; b) J. Liu, E. Sheina, T. Kowalewski, R. D. McCullough, *Angew. Chem. Int. Ed.* **2002**, 41, 329–332; *Angew. Chem.* **2002**, 114, 339–342.
 [6] a) Y. Shirota, *J. Mater. Chem.* **2000**, 10, 1–25; b) Y. Z. Su, J. T. Lin, Y. T. Tao, C. W. Ko, S. C. Lin, S. S. Sun, *Chem. Mater.* **2002**, 14, 1884–1890.
 [7] a) S. A. Ponomarenko, S. Kirchmeyer, A. Elschner, B. H. Huisman, A. Karbach, D. Dreschler, *Adv. Funct. Mater.* **2003**, 13, 591–596; b) Y. Nicolas, P. Blanchard, E. Levillain, M. Allain, N. Mercier, J. Roncali, *Org. Lett.* **2004**, 6, 273–276.
 [8] X. Xia, X. Fan, J. Locklin, R. C. Advincula, A. Gies, W. Nonidez, *J. Am. Chem. Soc.* **2004**, 126, 8735–8743.
 [9] M. Benabdellah, A. Aouniti, A. Dafali, B. Hammouti, M. Benkaddour, A. Yahyi, A. Ettouhami, *Appl. Surf. Sci.* **2005**, 252, 8341–8347.
 [10] F. A. Larik, M. Faisal, A. Saeed, Q. Abbas, M. A. Kazi, N. Abbas, A. A. Thebo, D. M. Khan, P. A. Channar, *J. Mater. Sci. Mater. Electron.* **2018**, 29, 17975–18010.
 [11] S. Anandan, S. Manoharan, N. K. S. Narendran, T. C. S. Girsun, A. M. Asiri, *Opt. Mater.* **2018**, 85, 18–25.
 [12] R. Mishra, P. K. Sharma, *Int. J. Eng. Al. Sci.* **2015**, 1, 46–59.
 [13] A. D. Pillai, P. D. Rathod, F. P. Xavier, H. Padh, V. Sudarsanam, K. K. Vasu, *Bioorg. Med. Chem.* **2005**, 13, 6685–6692.
 [14] T. Nasr, S. Bondock, S. Eid, *Eur. J. Med. Chem.* **2014**, 84, 491–504.
 [15] K. Jha, S. Kumar, I. Tomer, R. Mishra, *J. Pharm. Res.* **2012**, 5, 560–566.
 [16] R. Shah, P. K. Verma, *Chem. Cent. J.* **2018**, 12, 137.
 [17] G. Barbarella, M. Melucci, G. Sotgiu, *Adv. Mater.* **2005**, 17, 1581–1593.
 [18] N. Kushwaha, C. S. Sharma, *Mini-Rev. Med. Chem.* **2020**, 20, 2104–2122.
 [19] S. Debnath, G. Hao, B. Guan, P. Thapa, J. Hao, H. Hammers, X. Sun, *Int. J. Mol. Sci.* **2022**, 23, 7160.
 [20] H. Li, H. Zhou, S. Krieger, J. J. Parry, J. J. Whittenberg, A. V. Desai, B. E. Rogers, P. J. A. Kenis, D. E. Reichert, *Bioconjugate Chem.* **2014**, 25, 761–772.
 [21] T. J. Mooibroek, P. Gamez, *Inorg. Chim. Acta.* **2007**, 360, 381–404.
 [22] B. Klenke, M. Stewart, M. P. Barrett, R. Brun, I. H. Gilbert, *J. Med. Chem.* **2001**, 44, 3440–3452.
 [23] X. P. Hu, H. L. Chen, Z. Zheng, *Adv. Synth. Catal.* **2005**, 347, 541–548.
 [24] H. S. Patel, V. C. Patel, *Eur. Polym. J.* **2001**, 37, 2263–2271.
 [25] B. F. Abrahams, S. R. Batten, H. Hamit, B. F. Hoskins, R. Robson, *Chem. Commun.* **1996**, 1313–1314.
 [26] J. A. Zerkowski, C. T. Seto, G. M. Whitesides, *J. Am. Chem. Soc.* **1992**, 114, 5473–5475.
 [27] T. Hosokai, H. Muraoka, M. Mori, R. Kurihara, S. Ogawa, N. Yoshimoto, *Jpn. J. Appl. Phys.* **2014**, 53, 01AB15.
 [28] a) G. Barbarella, M. Zambianchi, A. Bongini, L. Antolini, *Adv. Mater.* **1993**, 5, 834–838; b) E. A. Marseglia, F. Grepioni, E. Tedesco, D. Braga, *Mol. Cryst. Liq. Cryst.* **2000**, 348, 137.
 [29] a) J. Roncali, *Chem. Rev.* **1997**, 97, 173–206; b) G. Zotti, G. Schiavon, S. Zecchin, L. Groenendaal, *Chem. Mater.* **1999**, 11, 3624–3628.
 [30] T. Kusukawa, M. Fujita, *J. Am. Chem. Soc.* **2002**, 124, 13576–13582.
 [31] T. Yasuda, T. Shimizu, F. Liu, G. Ungar, T. Kato, *J. Am. Chem. Soc.* **2011**, 133, 13437–13444.
 [32] J. Liu, K. Wang, F. Xu, Z. Tang, W. Zheng, J. Zhang, C. Li, T. Yu, X. You, *Tetrahedron Lett.* **2011**, 52, 6492–6496.
 [33] Z.-F. An, R.-F. Chen, J. Yin, G.-H. Xie, H.-F. Shi, T. Tsuboi, W. Huang, *Chem. Eur. J.* **2011**, 17, 10871–10878.
 [34] K. Li, Y. Jiang, D. Ding, X. Zhang, Y. Liu, J. Hua, S.-S. Feng, B. Liu, *Chem. Commun.* **2011**, 47, 7323–7325.
 [35] R. Kannan, G. S. He, T.-C. Lin, P. N. Prasad, R. A. Vaia, L.-S. Tan, *Chem. Mater.* **2004**, 16, 185–194.
 [36] B. S. Roczynski, J. M. Szarko, H. J. Son, L. Yu, L. X. Chen, *J. Phys. Chem. Lett.* **2014**, 5, 1856–1863.
 [37] J. H. Seo, T.-Q. Nguyen, *J. Am. Chem. Soc.* **2008**, 130, 10042–10043.
 [38] S. K. Das, P. Bhanja, S. K. Kundu, S. Mondal, A. Bhaumik, *ACS Appl. Mater. Interfaces* **2018**, 10, 23813–23824.
 [39] M. Saleh, H. M. Lee, K. C. Kemp, K. S. Kim, *ACS Appl. Mater. Interfaces* **2014**, 6, 7325–7333.
 [40] X. Zhuang, F. Zhang, D. Wu, N. Forler, H. Liang, M. Wagner, D. Gehrig, M. R. Hansen, F. Laquai, X. Feng, *Angew. Chem. Int. Ed.* **2013**, 52, 9668–9672; *Angew. Chem.* **2013**, 125, 9850–9854.
 [41] X. Feng, Y. Liang, L. Zhi, A. Thomas, D. Wu, I. Lieberwirth, U. Kolb, K. Mullen, *Adv. Funct. Mater.* **2009**, 19, 2125–2129.
 [42] J. Liang, Y. Jiao, M. Jaroniec, S. Z. Qiao, *Angew. Chem. Int. Ed.* **2012**, 51, 11496–11500; *Angew. Chem.* **2012**, 124, 11664–11668.
 [43] X. Wang, J. Wang, D. L. Wang, S. O. Dou, Z. L. Ma, J. H. Wu, L. Tao, A. L. Shen, C. B. Ouyang, Q. H. Liu, S. Y. Wang, *Chem. Commun.* **2014**, 50, 4839–4842.
 [44] Z. Xiang, D. Cao, L. Huang, J. Shui, M. Wang, L. Dai, *Adv. Mater.* **2014**, 26, 3315–3320.
 [45] J. H. Forsberg, V. T. Spaziano, S. P. Klump, K. M. Sanders, *J. Heterocycl. Chem.* **1988**, 25, 767–770.
 [46] F. Chérioux, L. Guyard, P. Audebert, *Chem. Commun.* **1998**, 2225–2226.
 [47] F. Chérioux, H. Maillotte, P. Audebert, J. Zyss, *Chem. Commun.* **1999**, 2083–2084.
 [48] A. de Meijere, F. Diederich, *Metal-Catalyzed Cross-Coupling Reactions*. 2nd ed. Wiley-VCH; Weinheim, Germany, **2004**.
 [49] C. C. S. Johansson, M. O. Kitching, T. L. Colacot, V. Snieckus, *Angew. Chem. Int. Ed.* **2012**, 51, 5062–5085; *Angew. Chem.* **2012**, 124, 5150–5174.
 [50] K. C. Nicolaou, P. G. Bulger, D. Sarlah, *Angew. Chem. Int. Ed.* **2005**, 44, 4442–4489; *Angew. Chem.* **2005**, 117, 4516–4563.
 [51] K. Zhao, L. Shen, Z.-L. Shen, T.-P. Loh, *Chem. Soc. Rev.* **2017**, 46, 586–602.
 [52] J. M. Gil-Negrete, J. P. Pérez Sestelo, L. A. Sarandeses, *Chem. Commun.* **2018**, 54, 1453–1456.

- [53] M. Giannerini, M. Fañanás-Mastral, B. L. Feringa, *Nat. Chem.* **2013**, *5*, 667–672.
- [54] C. E. I. Knappke, A. J. Wangelin, *Chem. Soc. Rev.* **2011**, *40*, 4948–4962.
- [55] P. Leriche, F. Piron, E. Ripaud, P. Frère, M. Allain, J. Roncali, *Tetrahedron Lett.* **2009**, *50*, 5673–5676.
- [56] A. Naka, R. Fukuda, R. Kishimoto, Y. Yamashita, Y. Ooyama, J. Ohshita, M. Ishikawa, *J. Organomet. Chem.* **2012**, *702*, 67–72.
- [57] T. Zhang, W. Liu, M. Wang, P. Liu, Y. Pan, D. Liu, *High Perform. Polym.* **2017**, *29*, 513–523.
- [58] M. Pasini, S. Destri, C. Botta, W. Porzio, *Synth. Met.* **2000**, *113*, 129–133.
- [59] a) J. Preat, D. Jacquemin, C. Michaux, E. A. Perpète, *Chem. Phys.* **2010**, *376*, 56–58; b) W. Zhu, G. S. Wu, *J. Phys. Chem. A* **2001**, *105*, 9568–9574.
- [60] R. Maragani, R. Misra, *Tetrahedron Lett.* **2013**, *54*, 5399–5402.
- [61] H. Muraoka, M. Mori, S. Ogawa, *Phosphorous Sulfur Silicon Relat. Elem.* **2015**, *190*, 1382–1391.
- [62] J. R. Schaefgen, P. J. Flory, *J. Am. Chem. Soc.* **1948**, *70*, 2709–2718.
- [63] M. Morton, T. E. Helminiak, S. D. Gadkary, F. Bueche, *J. Polym. Sci.* **1962**, *57*, 471–482.
- [64] B. Walker, C. Kim, T.-Q. Nguyen, *Chem. Mater.* **2011**, *23*, 470–482.
- [65] J. Roncali, *Acc. Chem. Res.* **2009**, *42*, 1719–1730.
- [66] Y. Lin, Y. Li, X. Zhan, *Chem. Soc. Rev.* **2012**, *41*, 4245–4272.
- [67] H. M. Diab, A. M. Abdelmoniem, M. R. Shaaban, I. A. Abdelhamid, A. H. M. Elwahy, *RSC Adv.* **2019**, *9*, 16606–16682.
- [68] S. Kotha, M. Meshram, N. R. Panguluri, V. R. Shah, S. Todeti, M. E. Shirbhate, *Chem. Asian J.* **2019**, *14*, 1356–1403.
- [69] K. Asai, G.-I. Konishi, K. Sumi, K. Mizuno, *J. Organomet. Chem.* **2011**, *696*, 1236–1243.
- [70] Y. P. Zhong, J. M. Gao, P. Liu, W. J. Deng, *Mater. Res. Innovations* **2015**, *19*, S51–S54.
- [71] a) P. N. Prasad, J. D. Bhawalkar, N. D. Kumar, M. Lal, *Macromol. Symp.* **1997**, *118*, 467–472; b) P. K. Frederiksen, M. Jørgensen, P. R. Ogilby, *J. Am. Chem. Soc.* **2001**, *123*, 1215–1221; c) P. K. Frederiksen, S. P. McIlroy, C. B. Nielsen, L. Nikolajsen, E. Skovsen, M. Jørgensen, K. V. Mikkelsen, P. R. Ogilby, *J. Am. Chem. Soc.* **2005**, *127*, 255–269; d) M. Khurana, H. A. Collins, A. Karotki, H. L. Anderson, D. T. Cramb, B. C. Wilson, *Photochem. Photobiol.* **2007**, *83*, 1441–1448.
- [72] a) J. D. Bhawalkar, G. S. He, P. N. Prasad, *Rep. Prog. Phys.* **1996**, *59*, 1041; b) C. W. Spangler, *J. Mater. Chem.* **1999**, *9*, 2013–2020; c) J. E. Ehrlich, X. L. Wu, L.-Y. Lee, Z.-Y. Hu, H. Rockel, S. R. Marder, J. W. Perry, *Opt. Lett.* **1997**, *22*, 1843–1845.
- [73] a) W. Denk, J. H. Strickler, W. W. Webb, *Science* **1990**, *248*, 73–76; b) C. Xu, W. R. Zipfel, J. B. Shear, R. M. Williams, W. W. Webb, *Proc. Natl. Acad. Sci. USA* **1996**, *93*, 10763–10768; c) R. H. Köhler, J. Cao, W. R. Zipfel, W. W. Webb, M. R. Hansen, *Science* **1997**, *276*, 2039–2042; d) H. M. Kim, B. R. Cho, *Acc. Chem. Res.* **2009**, *42*, 863–872.
- [74] a) B. H. Cumpston, S. P. Ananthavel, S. Barlow, D. L. Dyer, J. E. Ehrlich, L. L. Erskine, A. A. Heikal, S. M. Kuebler, I.-Y. S. Lee, D. McCord-Maughon, J. Qin, H. Röckel, M. Rumi, X.-L. Wu, S. R. Marder, J. W. Perry, *Nature* **1999**, *398*, 51–54; b) Y. Z. Shen, J. Swiatkiewicz, D. Jakubczyk, F. M. Xu, P. N. Prasad, R. A. Vaia, B. A. Reinhardt, *Appl. Opt.* **2001**, *40*, 938–940; c) D. A. Parthenopoulos, P. M. Rentzepis, *Science* **1989**, *245*, 843–845.
- [75] G. S. He, C. F. Zhao, J. D. Bhawalkar, P. N. Prasad, *Appl. Phys. Lett.* **1995**, *67*, 3703–3705.
- [76] Y. Cui, Q. Fang, G. Xue, G. Xu, L. Yin, W. Yu, *Chem. Lett.* **2005**, *34*, 644–645.
- [77] S. Liu, K. S. Lin, V. M. Churikov, Y. Z. Su, J. T. Lin, T.-H. Huang, C. C. Hsu, *Chem. Phys. Lett.* **2004**, *390*, 433–439.
- [78] F. Xu, Z. Wang, Q. Gong, *Opt. Mater.* **2007**, *29*, 723–727.
- [79] L. Zou, Z. Liu, X. Yan, Y. Liu, Y. Fu, J. Liu, Z. Huang, X. Chen, J. Qin, *Eur. J. Org. Chem.* **2009**, 5587–5593.
- [80] R. Misra, R. Maragani, C. P. Singh, R. Chari, *Dyes Pigm.* **2016**, *126*, 110–117.
- [81] a) Special Issue on “Supramolecular Chemistry and Self-Assembly”. *Science* **2002**, *295*, 2395–2421; b) Special Issue on “Supramolecular Approaches to Organic Electronics and Nanotechnology”. *Adv. Mater.* **2006**, *18*, 1227–1329.
- [82] a) L. C. Palmer, S. I. Stupp, *Acc. Chem. Res.* **2008**, *41*, 1674–1684; b) A. Ajayaghosh, V. K. Praveen, *Acc. Chem. Res.* **2007**, *40*, 644–656.
- [83] D. Demus, J. W. Goodby, G. W. Gray, H.-W. Spiess, V. Vill, *Handbook of Liquid Crystals*, Wiley-VCH, Weinheim, Germany, **1998**.
- [84] a) J. W. Goodby, I. M. Saez, S. J. Cowling, V. Görtz, M. Draper, A. W. Hall, S. Sia, G. Cosquer, S.-E. Lee, E. P. Raynes, *Angew. Chem. Int. Ed.* **2008**, *47*, 2754–2787; *Angew. Chem.* **2008**, *120*, 2794–2828; b) S. Laschat, A. Baro, N. Steinke, F. Giesselmann, C. Hägele, G. Scalia, R. Judele, E. Kapatsina, S. Sauer, A. Schreivogel, M. Tosoni, *Angew. Chem. Int. Ed.* **2007**, *46*, 4832–4887; *Angew. Chem.* **2007**, *119*, 4916–4973.
- [85] a) I. Nenner, G. J. J. Schultz, *Chem. Phys.* **1975**, *62*, 1747–1758; b) K. D. Jordan, P. D. Burrow, *Acc. Chem. Res.* **1978**, *11*, 341–348; c) L. Barrio, J. Catalan, J. L. G. de Paz, *Int. J. Quantum Chem.* **2003**, *91*, 432–437; d) P. F. H. Schwab, J. R. Smith, J. Michl, *Chem. Rev.* **2005**, *105*, 1197–1280.
- [86] T. Yasuda, T. Shimizu, F. Liu, G. Ungar, T. Kato, *J. Am. Chem. Soc.* **2011**, *133*, 13437–13444.
- [87] S.-H. Liao, J.-R. Shiu, S.-W. Liu, S.-J. Yeh, Y.-H. Chen, Y.-H. C.-T. Chen, T.-J. Chow, C.-I. Wu, *J. Am. Chem. Soc.* **2009**, *131*, 763–777.
- [88] H. Taing, J. G. Rothera, J. F. Binder, C. L. B. Macdonald, S. H. Eichhorn, *Liq. Cryst.* **2017**, *45*, 1147–1154.
- [89] K. Do, H. Choi, K. Lim, H. Jo, J. W. Cho, M. K. Nazeeruddin, J. Ko, *Chem. Commun.* **2014**, *50*, 10971–10974.
- [90] M. Deng, G. Zhang, L. Yu, X. Xu, Q. Peng, *Chem. Eng. J.* **2021**, *426*, 131910–131917.
- [91] T. Zhang, W. Liu, M. Wang, P. Liu, Y. Pan, D. Liu, *Polym. Degrad. Stab.* **2016**, *130*, 257–263.
- [92] T. Zhang, W. Liu, M. Wang, P. Liu, Y. Pan, D. Liu, *High Perform. Polym.* **2017**, *29*, 513–523.
- [93] H. Muraoka, H. Sasaki, S. Ogawa, *Bull. Chem. Soc. Jpn.* **2019**, *92*, 797–806.
- [94] H. K. Park, M. G. Ham, Y.-J. Kim, K. Takeuchi, J.-C. Choi, *J. Coord. Chem.* **2022**, *75*, 385–400.
- [95] L. Zou, Y. Fu, X. Yan, X. Chen, J. Qin, *J. Polym. Sci. Part A* **2008**, *46*, 702–712.
- [96] I. F. A. Mariz, E. M. S. Maçôas, J. M. G. Martinho, L. Zou, P. Zhou, X. Chen, J. Qin, *J. Mater. Chem. B* **2013**, *1*, 2169–2177.
- [97] L. Zou, Y. Liu, N. Ma, E. Maçôas, J. M. G. Martinho, M. Petterson, X. Chen, J. Qin, *Phys. Chem. Chem. Phys.* **2011**, *13*, 8838–8846.
- [98] P. Zhou, C. Zhong, X. Chen, J. Qin, I. Mariz, E. Maçôas, *Macromolecules* **2014**, *47*, 6679–6686.
- [99] M. G. Mohamed, A. F. M. EL-Mahdy, M. G. Kotp, S.-W. Kuo *Mater Adv* **2022**, *3*, 707–733.
- [100] Y. Zhang, S. N. Riduan, *Chem. Soc. Rev.* **2012**, *41*, 2083–2094.
- [101] T. Zhang, G. Xing, W. Chen, L. Chen, *Mater. Chem. Front.* **2020**, *4*, 332–353.
- [102] D.-H. Yang, Y. Tao, X. Ding, B.-H. Han, *Chem. Soc. Rev.* **2022**, *51*, 761–791.
- [103] S. K. Kundu, A. Bhaumik, *ACS Sustainable Chem. Eng.* **2016**, *4*, 3697–3703.
- [104] Z. Wang, J. Liu, Y. Fu, C. Liu, C. Pan, Z. Liu, G. Yu, *Chem. Commun.* **2017**, *53*, 4128–4131.
- [105] N. R. Kumar, P. Das, A. R. Agrawal, S. K. Mandal, S. S. Zade, *Mater Adv* **2021**, *2*, 7473–7481.
- [106] N. Das, R. Paul, D. Q. Dao, R. Chatterjee, K. Borah, S. C. Shit, J. Mondal, *ACS Appl. Nano Mater.* **2022**, *5*, 5302–5315.
- [107] N. Bakhtiari, S. Azizian, S. M. Alshehri, N. L. Torad, V. Malgras, Y. Yamauchi, *Microporous Mesoporous Mater.* **2015**, *217*, 173–177.
- [108] S. Wang, Y. Peng, *Chem. Eng. J.* **2010**, *156*, 11–24.
- [109] H. H. Najafabadi, M. Irani, L. R. Rad, A. H. Haratameh, I. Haririan, *RSC Adv.* **2015**, *5*, 16532–16539.
- [110] S. Zhu, N. Yang, D. Zhang, *Mater. Chem. Phys.* **2009**, *113*, 784–789.
- [111] E. G. Deze, S. K. Papageorgiou, E. P. Favvas, F. K. Katsaros, *Chem. Eng. J.* **2012**, *209*, 537–546.
- [112] W. S. Ngah, S. Fatinathan, *J. Environ. Manage.* **2010**, *91*, 958–969.
- [113] D. Wu, F. Xu, B. Sun, R. Fu, H. He, K. Matyjaszewski, *Chem. Rev.* **2012**, *112*, 3959–4015.
- [114] R. J. Angelici, *Coord. Chem. Rev.* **1990**, *105*, 61–76.
- [115] K. Hara, M. Kurashige, Y. Dan-oh, C. Kasada, A. Shinpo, S. Suga, K. Sayama, H. Arakawa, *New J. Chem.* **2003**, *27*, 783–785.
- [116] A. Morita, T. Yamamoto, Y. Miyazaki, T. Maruyama, H. Wakayama, Z. Zhou, Y. Nakamura, T. Kanbara, *Macromolecules* **1992**, *25*, 1214–1223.
- [117] Y. N. Sum, M. X. Tan, J. Y. Ying, Y. Zhang, *Energy Environ. Sci.* **2013**, *6*, 3254–3259.
- [118] Y. He, Q. Liu, F. Liu, C. Huang, C. Peng, Q. Yang, H. Wang, J. Hu, H. Liu, *Microporous Mesoporous Mater.* **2016**, *233*, 10–15.
- [119] D.-Y. Wang, W.-J. Wang, R. Wang, S.-C. Xi, B. Dong, *Eur. Polym. J.* **2021**, *147*, 110297.
- [120] S. Park, M.-S. Kim, W. Jang, J. K. Park, D. H. Wang, *Nanoscale* **2018**, *10*, 4708–4717.
- [121] Q. Fu, T. Wang, Y. Sun, N. Zheng, Z. Xie, D. Lu, Z. Xu, X. Wan, Y. Zhang, Y. Liu, *Sci. China Chem.* **2021**, *64*, 82–91.

- [122] Y. Zhi, S. Ma, H. Xia, Y. Zhang, Z. Shi, Y. Mu, X. Liu, *Appl. Catal. B* **2019**, *244*, 36–44.
- [123] X. Yuan, D. Dragoe, P. Beauvier, D. B. Uribe, L. Ramos, M. G. Mendez-Medrano, H. Remita, *J. Mater. Chem. A* **2020**, *8*, 268–277.
- [124] Z. J. Wang, K. Garth, S. Ghasimi, K. Landfester, K. A. I. Zhang, *ChemSusChem* **2015**, *8*, 3459–3464.
- [125] W. Huang, J. Byun, I. Rörich, C. Ramanan, P. W. M. Blom, H. Lu, D. Wang, L. C. da Silva, R. Li, L. Wang, K. Landfester, K. A. I. Zhang, *Angew. Chem. Int. Ed.* **2018**, *57*, 8316–8320.
- [126] H. Bohra, P. Li, C. Yang, Y. Zhao, M. Wang, *Polym. Chem.* **2018**, *9*, 1972–1982.
- [127] S. K. Kundu, A. Kayet, R. Baidya, L. Satyanarayan, D. K. Maiti, *ACS Omega* **2020**, *5*, 394–405.
- [128] J. Wang, G. Ouyang, Y. Wang, X. Qiao, W.-S. Li, H. Li, *Chem. Commun.* **2020**, *56*, 1601–1604.
- [129] X. Lan, Q. Li, Y. Zhang, Q. Li, L. R. Sandoval, G. Bai, *Appl. Catal. B* **2020**, *277*, 119274–119285.
- [130] Y. Du, H. Liu, *ChemCatChem* **2021**, *13*, 5178–5190.
- [131] B. Chen, L. Chen, Z. Yan, J. Kang, S. Chen, Y. Jin, L. Ma, C. Xia, *Green Chem.* **2021**, *23*, 3607–3611.
- [132] X. Han, Y. Zhang, Y. Dong, J. Zhao, S. Ming, J. Zhang, *RSC Adv.* **2022**, *12*, 708–718.
- [133] Q. Sheng, X. Zhong, Q. Shang, Y. Dong, J. Zhao, Y. Du, Y. Xie, *Front. Chem.* **2022**, *10*, 854018.
- [134] Z. Xiang, D. Cao, L. Huang, J. Shui, M. Wang, L. Dai, *Adv. Mater.* **2014**, *26*, 3315–3320.
- [135] Y. Xu, S. Jin, H. Xu, A. Nagai, D. Jiang, *Chem. Soc. Rev.* **2013**, *42*, 8012–8031.
- [136] M. E. Bhosale, R. Illathvalappil, S. Kurungot, K. Krishnamoorthy, *Chem. Commun.* **2016**, *52*, 316–318.
- [137] a) M.-S. Kim, C. S. Phang, Y. K. Jeong, J. K. Park, *Polym. Chem.* **2017**, *8*, 5655–5659; b) M.-S. Kim, W.-J. Lee, S.-M. Paek, J. K. Park, *ACS Appl. Mater. Interfaces* **2018**, *10*, 32102–32111.
- [138] M.-S. Kim, M. Lee, M.-J. Kim, Y. K. Jeong, J. K. Park, S.-M. Paek, *J. Mater. Chem. A* **2020**, *8*, 17790–17799.
- [139] X. Liu, S. Wang, A. Wang, J. Chen, Z. Wang, Q. Zeng, W. Liu, Z. Li, L. Zhang, *J. Phys. Chem. C* **2019**, *123*, 21327–21335.
- [140] S.-B. Ren, W. Ma, C. Zhang, L. Chen, K. Wang, R.-R. Li, M. Shen, D.-M. Han, Y. Chen, J.-X. Jiang, *ChemSusChem* **2020**, *13*, 2295–2302.
- [141] Y. Zhang, H. Lv, Z. Zhang, L. Wang, X. Wu, H. Xu, *Adv. Mater.* **2021**, *33*, 2008264.
- [142] Y. S. Kochergin, S. M. B. Mousavi, B. Khezri, P. Lyu, M. J. Bojdys, M. Pumera, *J. Mater. Chem. A* **2021**, *9*, 7162–7171.
- [143] X. Xue, J. Luo, L. Kong, J. Zhao, Y. Zhang, H. Du, C. Shuang, Y. Xie, *RSC Adv.* **2021**, *11*, 10688–10698.
- [144] —S. Chen, S. Wang, X. Xue, J. Zhao, H. Du, *Polymer.* **2021**, *13*, 3300.
- [145] H. Chai, S. Wang, X. Wang, J. Ma, J. Jin, *ACS Catal.* **2022**, *12*, 3700–3709.

Manuscript received: September 15, 2022

Revised manuscript received: November 30, 2022